UC Berkeley
UC Berkeley Previously Published Works

Title
Bilayer nonlocal flat optics

Permalink
https://escholarship.org/uc/item/6kd8962m

Journal
eLight, 6(1)

ISSN
2097-1710

Authors
Tang, Haoning
Fan, Shanhui
Jie, Yao
et al.

Publication Date
2026-12-01

DOI
10.1186/s43593-026-00135-y

Copyright Information
This work is made available under the terms of a Creative Commons Attribution License, available at https://creativecommons.org/licenses/by/4.0/

Peer reviewed

eScholarship.org Powered by the California Digital Library
University of California

REVIEW Open Access

Bilayer nonlocal flat optics

Haoning Tang[1,2*], Shanhui Fan[3,4], Yao Jie[5,6,7], Hai Son Nguyen[8,9], Eric Mazur[10,11] and Yuan Cao[2,7,12]

Abstract

Nonlocal flat optics such as photonic crystal slabs, guided-resonance dielectric metasurfaces, and plasmonic lattices use collective Bloch modes and their radiation coupling to achieve sharp spectral selectivity, tailored dispersion, and wavefront control within subwavelength thicknesses. Yet in single-layer platforms, optical functionality is constrained by limited geometric degrees of freedom: in-plane symmetry and pre-patterned geometry largely determine mode structure, while radiation channels, linewidths, and polarization responses are often linked through fixed symmetry-imposed selection rules. Bilayer nonlocal flat-optics platforms break this bottleneck by introducing interlayer degrees of freedom that are independent of the in-plane lattice design, most importantly the interlayer separation (controlling near-field hybridization strength and far-field interference phase), as well as relative translation, twist, and lattice mismatch. This review organizes bilayer nonlocal flat optics by interlayer configurations and highlights the additional design space and reconfigurability uniquely enabled by two coupled flat-optical layers. For example, we connect aligned bilayers to mode hybridization, radiation interference, and high-Q routes to bound states in the continuum. We then show how lateral misalignment unlocks symmetry breaking, off-Γ singularities, unidirectional guided resonances, and synthetic-dimensional non-Hermitian topology. Next, we discuss how lattice mismatch generates moiré superlattices with miniband flattening and localization into moiré cavities, and how twist-driven momentum mixing supports twist-tunable resonances, moiré quasi-BICs, structured radiation such as optical vortices, beam steering, and emergent chirality. Across these themes, bilayer systems unify band-structure engineering, radiation-channel topology, and post-fabrication tunability into a compact platform for reconfigurable flat-optical devices.

*Correspondence:
Haoning Tang
haoning@mit.edu
[1] Department of Mechanical Engineering, Massachusetts Institute of Technology, Cambridge, MA 02139, USA
[2] Department of Electrical Engineering and Computer Science, University of California at Berkeley, Berkeley, CA 94720, USA
[3] Electrical Engineering Department, Stanford University, Stanford, CA 94305, USA
[4] Department of Applied Physics and Ginzton Laboratory, Stanford University, Stanford, CA, USA
[5] Department of Materials Science and Engineering, University of California, Berkeley, CA 94720, USA
[6] Applied Science and Technology Graduate Group, University of California, Berkeley, CA 94720, USA
[7] Lawrence Berkeley National Laboratory, Berkeley, CA 94720, USA
[8] CNRS-International-NTU-Thales Research Alliance (CINTRA), IRL 3288, Singapore 637553, Singapore
[9] UMR5270, Ecole Centrale de Lyon, INSA Lyon, Université Claude Bernard Lyon 1, CPE Lyon, CNRS, INL, 69130 Ecully, France
[10] School of Engineering and Applied Sciences, Harvard University, Cambridge, MA 02138, USA
[11] Department of Physics, Harvard University, Cambridge, MA 02138, USA
[12] Department of Physics, University of California at Berkeley, Berkeley, CA 94720, USA

© The Author(s) 2026. **Open Access** This article is licensed under a Creative Commons Attribution 4.0 International License, which permits use, sharing, adaptation, distribution and reproduction in any medium or format, as long as you give appropriate credit to the original author(s) and the source, provide a link to the Creative Commons licence, and indicate if changes were made. The images or other third party material in this article are included in the article's Creative Commons licence, unless indicated otherwise in a credit line to the material. If material is not included in the article's Creative Commons licence and your intended use is not permitted by statutory regulation or exceeds the permitted use, you will need to obtain permission directly from the copyright holder. To view a copy of this licence, visit http://creativecommons.org/licenses/by/4.0/.

1 Introduction

Flat optics have transformed how light is shaped by replacing bulky refractive components with subwavelength-thick nanostructured layers. Within this broad landscape, nonlocal flat optics occupy a distinctive and increasingly important regime. Rather than treating each unit cell as an isolated meta-atom, nonlocal platforms (e.g., photonic crystal slabs, dielectric guided resonance metasurfaces, and periodic plasmonic lattices) derive their optical responses from collective Bloch modes that extend across many periods. This nonlocality enables sharp spectral features, strong dispersion engineering, and radiation control, often mediated by guided resonances that couple to free-space channels and produce Fano lineshapes [1].

Nonlocal flat optics are therefore naturally described in a coupled-mode and scattering language: dispersion, symmetry, and the availability of radiative channels jointly determine which modes can be excited, how strongly they leak, and what wavefront or polarization pattern emerges in the far field [2, 3]. This viewpoint has led to a rich set of phenomena such as bound states in the continuum (BICs), quasi-BICs, polarization singularities, engineered effective indices, and non-Hermitian band topology [4]. Many of these phenomena are difficult to realize in purely local metasurfaces. At the same time, the simplicity of monolayer flat-optics platforms also limits the available degrees of freedom. In a single patterned layer, the key knobs are predominantly in-plane: unit-cell geometry, lattice symmetry, and thickness. As a result, design targets that simultaneously demand narrow linewidth (high-Q resonance), programmable radiation directionality, polarization selectivity or chirality, and reconfigurability often face hard trade-offs because they compete through the same symmetry-controlled radiation pathways.

Bilayer nonlocal flat optics (Fig. 1a) offers a clean way to add new and largely independent control parameters without abandoning planar fabrication. By stacking two flat optical layers into a single structure with coupled electromagnetic fields, one introduces interlayer degrees of freedom (interlayer separation, lateral translation (sliding) between layers, twist angle, and even lattice mismatch) that reorganize near-field mode hybridization and far-field radiation coupling in ways that are not accessible to monolayers. Importantly, these interlayer parameters are also natural candidates for reconfigurability.

These interlayer degrees of freedom can be understood through three recurring mechanisms: near-field hybridization, far-field radiative coupling, and momentum selection or mixing. These mechanisms are related but distinct. (Fig. 1b) Near-field hybridization describes direct coupling between resonant eigenmodes and mainly controls frequency splitting, band renormalization, and mode profiles. Far-field radiative coupling describes coupling through a shared radiation continuum and mainly controls linewidth, directionality, and BIC or quasi-BIC formation. Momentum selection and mixing determine which modes and radiation channels are allowed to interact in the first place.

In aligned bilayers, the interlayer gap d controls both near-field hybridization and the radiative phase delay between the two layers, leading to superradiant and subradiant resonances, as well as symmetry-protected and Fabry–Pérot-type bound states in the continuum. Lateral displacement breaks selected symmetries while preserving periodicity, thereby converting symmetry-protected BICs into quasi-BICs and rephasing the radiation channels. Lattice mismatch and global twist introduce moiré supercells and rotated reciprocal lattices, producing miniband folding, flat-band localization, twist-tunable resonances, and structured far-field radiation. Local twist instead acts within the unit cell, generating bianisotropy, chirality, and polarization-selective resonances without requiring a large moiré supercell. Table 1 provides a compact roadmap of the corresponding knobs, mechanisms, and representative applications.

Although Fig. 1 is organized by interlayer geometry, the same physical mechanisms can be realized across several material platforms. Dielectric photonic-crystal slabs and guided-resonance dielectric metasurfaces are natural platforms for high-Q guided resonances, BIC-derived leakage suppression, and dispersion engineering. Plasmonic lattices and metasurfaces instead emphasize strong local fields, collective surface-lattice resonances, and gain-assisted emission, but they are more strongly affected by Ohmic loss. Active and nonlinear platforms further extend the same design logic to lasing, frequency conversion, and quantum-emitter coupling. Thus, the material platform mainly changes the balance among near-field confinement, radiative leakage, absorption, gain, and fabrication tolerance, while the organizing knobs, such as spacing, translation, twist, and mismatch, remain broadly applicable.

The rest of this Review follows this organization. Section 2 discusses aligned bilayers and vertical coupling; Sect. 3 treats lateral displacement; Sects. 4 and 5 discuss lattice-mismatched and globally twisted moiré systems; Sect. 6 focuses on locally twisted bilayers; and Sect. 7 extends the discussion to multilayer stacks.

2 Coupled bilayer flat optics

2.1 Single-layer guided resonances and radiative channels

Many periodic nonlocal flat-optics structures, such as photonic crystal (PhC) slabs, can be described using Bloch-mode theory (Fig. 2a) [5]. Because these structures

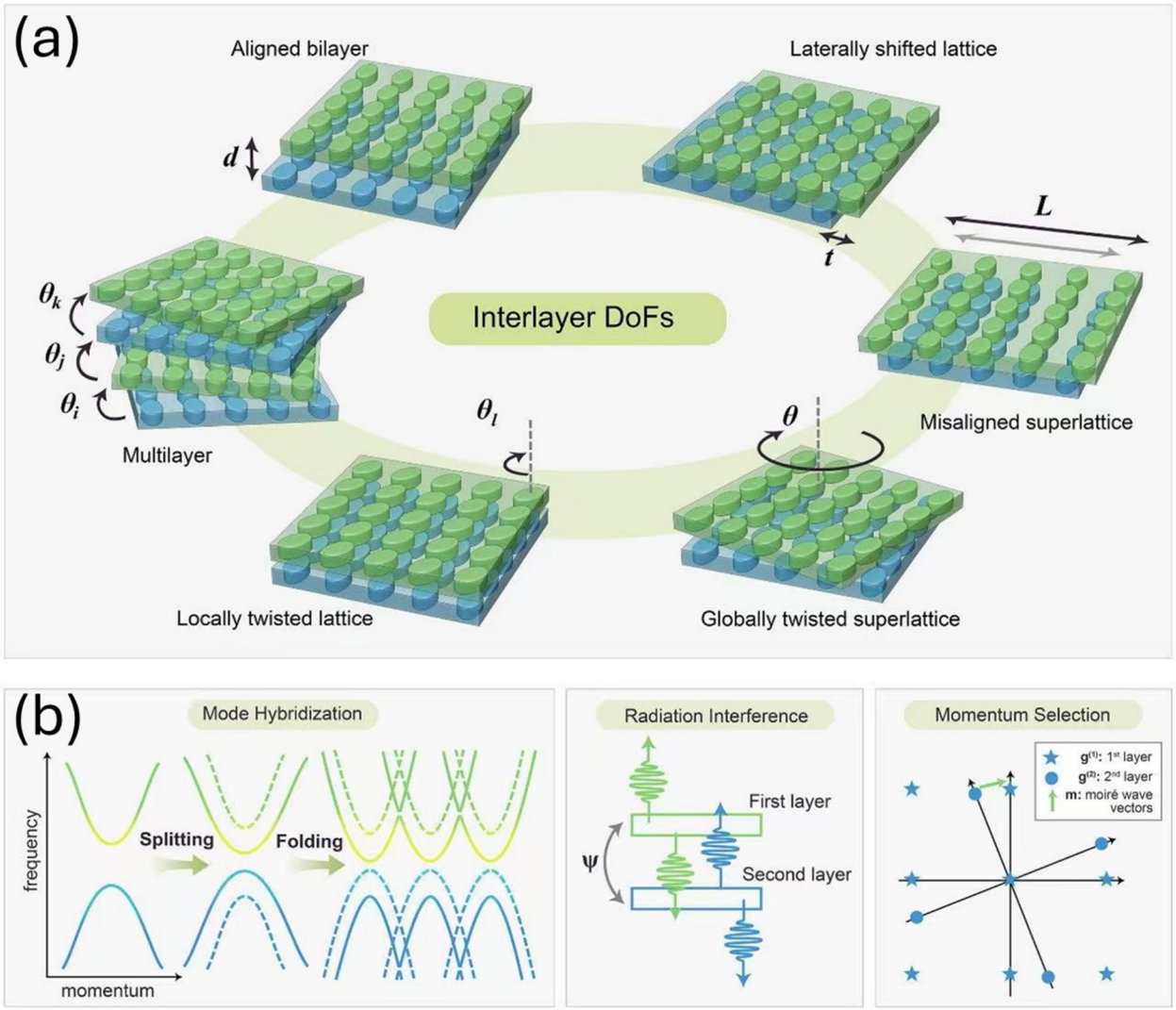


Fig. 1 Interlayer degrees of freedom that organize reconfigurable bilayer and multilayer nonlocal flat optics. **a** Schematic of coupled-layer configurations in which the in-plane lattice is fixed, while interlayer geometry provides largely independent knobs for mode hybridization and radiation control. In an aligned bilayer flat optics, the two identical lattices are separated by an interlayer distance d. In a laterally shifted bilayer flat optics, a translation t preserves periodicity but breaks mirror symmetry. In bilayer misaligned flat optics, a lattice mismatch given by L generates a long-period misaligned (moiré) superlattice in one dimension. In twisted bilayer flat optics, a global twist θ rotates the reciprocal lattices and creates two-dimensional (moiré) superlattice. In a locally twisted bilayer flat optics, the local twist θ_ℓ creates mismatch within one unit cell without changing the periodicity. In multilayer flat optics, each layer is twisted by $\{\theta_j\}$. These geometric configurations can be implemented across multiple nonlocal flat-optics platforms, including dielectric photonic-crystal slabs, guided-resonance dielectric metasurfaces, plasmonic lattices, and active or nonlinear multilayer structures. The same interlayer mechanisms apply broadly, although the dominant trade-offs among Q, mode volume, radiative coupling, material absorption, gain, and fabrication tolerance are platform dependent. **b** Conceptual illustration of the three core physical mechanisms through which bilayer coupling modifies nonlocal optical responses: (left) near-field mode hybridization, where coupling between layers splits and reshapes the dispersion of Bloch resonances; (middle) far-field radiation interference, where the two layers radiate into the same continuum and interfere to produce super- and sub-radiant states, including BICs; and (right) momentum selection and mixing, where rotated or mismatched reciprocal lattices introduce additional scattering channels and enable moiré-assisted momentum conversion

are subwavelength-thick in the out-of-plane direction, their Bloch modes can either remain guided or couple to free-space radiation. Modes outside the light cone are true guided modes, whereas modes inside the light cone overlap with the radiation continuum and become guided resonances, or leaky modes. These guided resonances typically appear as Fano features in transmission or reflection spectra.

At high-symmetry points, most notably the Γ-point under normal incidence, the coupling between a Bloch

Table 1 Summary of interlayer control knobs, mechanisms, and representative functions in bilayer and multilayer nonlocal flat optics

Configuration	Key mechanism	Representative functions
Aligned bilayer	Hybridization and radiation interference controlled by d	Mode splitting, SP-/FP-BICs, high-Q filtering and modulation
Laterally shifted bilayer	Symmetry breaking and radiation rephasing controlled by Δx, Δy	Quasi-BICs, off-Γ singularities, UGRs, spatiotemporal vortices
Lattice-mismatched bilayer	Moiré miniband folding and momentum mixing controlled by L	Flat bands, moiré cavities, slow light, enhanced density of states
Globally twisted bilayer	Moiré miniband folding and momentum mixing controlled by θ	Flat bands, moiré cavities, twist-tunable resonances, optical vortices, beam steering, chiral emission
Locally twisted bilayer	Unit-cell bianisotropy from rotated meta-atoms controlled by θ_ℓ	Optical activity, chiral quasi-BICs, circular dichroism, polarization control
Multilayer stack	Coupled-resonator network and cascaded phase control	Broadband response, nonlinear phase matching, cascaded chirality, hybrid flat bands

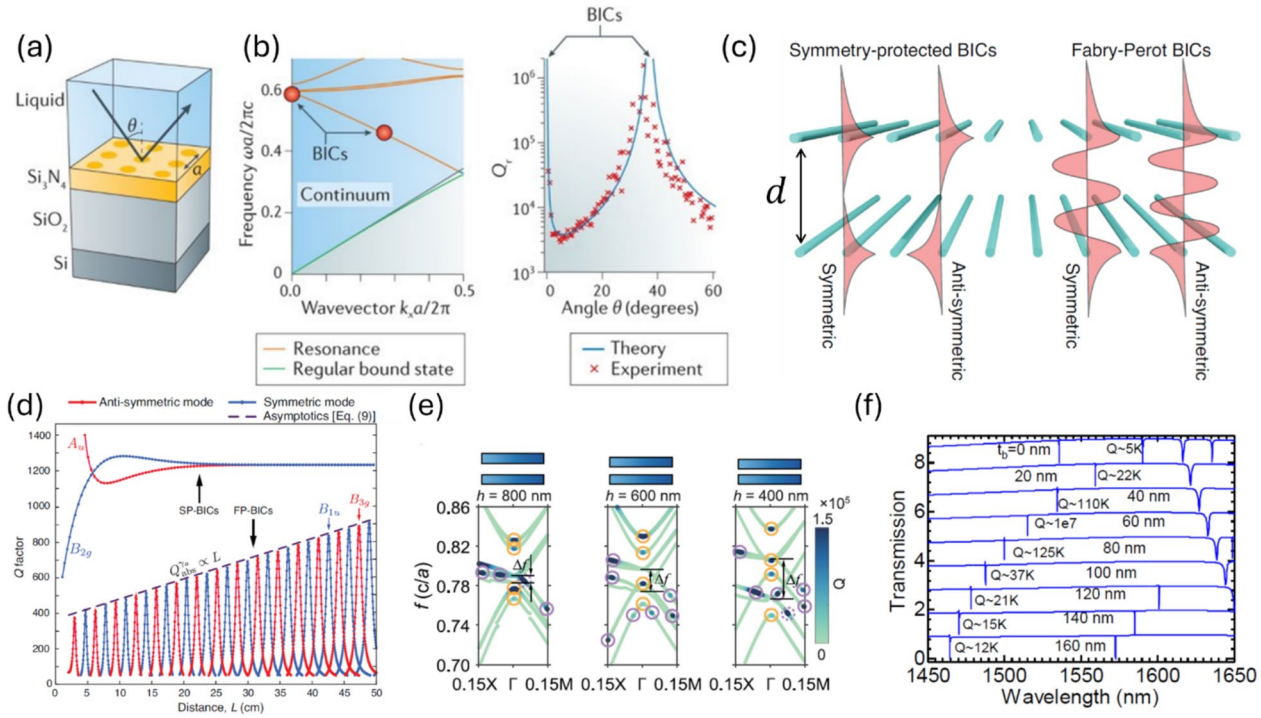


Fig. 2 Coupled bilayer flat optics: from guided resonances to reconfigurable BICs and high-Q modes. **a** Schematic of a single photonic crystal (PhC) slab on a substrate. Periodic patterning folds slab guided modes into the light cone, enabling radiative guided resonances. **b** Representative calculated band structure of a PhC slab showing guided resonances (orange) interacting with the radiation continuum (blue). At high-symmetry points, symmetry constraints suppress radiation, producing bound states in the continuum (BICs), as highlighted by the divergence of the radiative quality factor Q_r in theory and experiment [4]. **c** Classification of high-Q routes in aligned bilayer flat optics. Coupling between the two layers forms symmetric and antisymmetric supermodes, but these branches are not automatically both BICs. A branch becomes an SP-BIC when its symmetry representation is incompatible with the open radiation channel; a branch becomes an FP-BIC when the radiation amplitudes from the two layers destructively interfere at a specific interlayer phase. The bright partner generally remains radiative unless it satisfies an additional symmetry or interference condition [6]. **d** Numerically calculated Q-factors of symmetric and antisymmetric quasi-BICs as a function of interlayer distance d, illustrating the coexistence of SP-BICs (robust against d) and FP-BICs (periodic in d through radiative-phase interference) [6]. **e** Numerically calculated evolution of the bilayer PhC slab band structure as the interlayer gap h is varied. Interlayer coupling splits monolayer resonances into symmetric and antisymmetric branches with a frequency separation $\Delta f(d)$. Yellow and purple markers indicate SP-BICs and FP-BICs, respectively, highlighting their distinct dispersion behavior [9]. **f** Simulated transmission spectra of a representative double-layer PhC device for different buffer-layer thicknesses t_b. Increasing t_b tunes the radiative interference between the two layers, leading to pronounced linewidth narrowing and high-Q resonances without altering the in-plane geometry [22]. Panels **a** and **b** are reprinted with permission from Ref. [4] Copyright 2016, Springer Nature. Panels **c**, **d** are reprinted with permission from Ref. [6] Copyright 2026 by the American Physical Society. Panel **e** is reprinted with permission from Ref. [9]. Copyright 2024 by the American Physical Society. Panels **f** are reprinted with permission from Ref. [22]. © Optical Society of America

mode and open radiative channels is strongly constrained by symmetry (Fig. 2b). A useful criterion is whether the mode has a nonzero zeroth-order Fourier component, or spatial average, that can overlap with a normally incident plane wave. If the Bloch mode belongs to an irreducible representation that is incompatible with the incident plane-wave channel, this spatial average vanishes. As a result, the coupling matrix element to the corresponding free-space radiation channel is zero, producing a symmetry-protected bound state in the continuum (SP-BIC) [4, 6, 7].

While a SP-BIC is enforced by a symmetry mismatch between the optical mode and the accessible radiation channel, in contrast, a Fabry–Pérot or Friedrich–Wintgen-type BIC (FP-BIC) [7] is an interference-based BIC: the individual resonant pathways can radiate, but their outgoing radiation amplitudes cancel under a specific phase condition. When the symmetry or interference condition is imperfect, an ideal BIC becomes a quasi-BIC with a finite linewidth and a large but finite Q. Thus, SP-BICs and FP-BICs are parallel categories classified by their protection mechanism. They can coexist or merge in parameter space, but one does not generally contain the other. In multilayer structures, the same distinction remains useful: symmetry selection rules can persist if the full stack preserves the relevant symmetry, whereas interference-based BICs depend on phase cancellation among multiple radiative pathways.

2.2 Mode hybridization in aligned bilayers

We start our discussion with the aligned bilayer flat optics consisting of two photonic crystal (PhC) slabs stacked on top of each other. We first consider two identical patterned layers with no lateral displacement and no twist. Compared with a single layer, this geometry preserves all in-plane lattice symmetries but introduces one new control knob: the interlayer separation (spacer thickness), denoted here as d. (Fig. 2c) Crucially, d controls the coupling of Bloch modes in bilayer slabs in two complementary ways [6, 8–10]: 1. Near-field (evanescent) coupling sets the hybridization strength between guided resonances and decays rapidly with increasing d. 2. Far-field (radiative-channel) coupling adds a propagation phase $\phi \sim \omega d/c$ between layers, which enables radiative interference and Fabry–Pérot type background shaping.

In an aligned bilayer, the symmetry-selection rules for BICs are the same as those in the single-layer case. These rules now apply to paired (two-layer) eigenstates built from the same in-plane Bloch momentum. Because the two lattices are identical and strictly aligned, the in-plane translation symmetry is retained, and the in-plane momentum is conserved. In a coupled-mode description, interlayer tunneling therefore occurs only between single-layer modes with the same in-plane wavevector[9, 11] As a result, for the two-layer systems, such a coupling results in a pair of symmetric (bonding) and antisymmetric (antibonding) supermodes at a given frequency and momentum $(\omega, \mathrm{k}_{\parallel})$, with eigenfrequency shifts or splittings [8, 9, 12, 13]. The shifts and splittings are controlled by the coupling strength set by d.

2.3 High-Q points in bilayer flat-optics and dispersion tuning

Both SP-BICs and FP-BICs can produce high-Q states in aligned bilayer flat optics, but their physical origins are different. SP-BICs are inherited from the symmetry-selection rules of the single-layer structure. If the aligned bilayer preserves the relevant in-plane point-group symmetry, vertical mirror or layer-exchange symmetry, and in-plane momentum conservation, the coupled bilayer supermodes retain the same symmetry mismatch with the normally incident radiation channels. In this sense, bilayer SP-BICs are paired supermodes derived from single-layer SP-BICs rather than a separate class of BICs. Their existence does not require precise tuning of the interlayer separation d, although their frequencies and modal splittings can still vary with d.

By contrast, FP-BICs are interference-based BICs. Each layer, or each resonant pathway, can radiate by itself, but the total outgoing radiation amplitude can vanish when the interlayer propagation phase and resonant coupling satisfy a specific condition. Therefore, FP-BICs are accidental or interference-quantized BICs and are generally sensitive to d and background phase [6, 9, 14–19]. The interference-based FP-BIC route can be described compactly using a 2×2 non-Hermitian effective Hamiltonian that includes both near-field coupling and far-field radiative coupling [20, 21]

$$\widehat{H} = \begin{pmatrix} \omega_1 & \kappa \\ \kappa & \omega_2 \end{pmatrix} - i \begin{pmatrix} \gamma_1 & e^{i(\phi+\phi_1)}\sqrt{\gamma_1\gamma_2} \\ e^{i\phi+\phi_2}\sqrt{\gamma_1\gamma_2} & \gamma_2 \end{pmatrix},$$

where κ describes near-field coupling that strongly depends on d, $\gamma_{1,2}$ are radiative loss rates, $\omega_{1,2}$ are the resonance frequencies of the two isolated layers and $\phi \sim \omega d/c$ and $\phi_{1,2} \sim \omega t_{1,2}/c$ denote the interlayer and intralayer propagation phases, respectively, with $t_{1,2}$ the layer thicknesses. In the perfectly aligned case, the eigenvectors reduce to symmetric/antisymmetric combinations, but their linewidths can differ dramatically due to radiation interference, producing both enhanced leakage and suppressed leakage pair. As a result, a BIC condition emerges naturally from destructive interference in the radiative term, including the phase

requirements $e^{2i(\phi+\phi_1)} = e^{2i(\phi+\phi_2)} = 1$, together with the coupling constraint $\frac{|\omega_1-\omega_2|}{\kappa} = \left|\sqrt{\frac{\gamma_1}{\gamma_2}} - \sqrt{\frac{\gamma_2}{\gamma_1}}\right|$ [21]. In the case of identical layers ($\omega_1 = \omega_2$, $\gamma_1 = \gamma_2$, $\phi_1 = \phi_2$), the coupling constraint becomes trivial and the phase requirement is reduced to quantized condition of $\phi = \phi_0 + \pi m$. In such a configuration, the BIC is of FP-type and occurs at quantized distances d_m (often expressed as $\sim \pi mc/\omega_0$ near a target resonance ω_0).

A small deviation converts them into quasi-FP-BICs with finite Q. This sensitivity can be estimated from the phase detuning between the radiation emitted by the two layers. Near an FP-BIC at $d = d_{\mathrm{BIC}}$, a spacing error Δd produces a radiative phase mismatch $\Delta\phi \simeq 2k_z\Delta d \simeq 4\pi n_{\mathrm{gap}}\Delta d/\lambda_0$, where n_{gap} is the effective refractive index of the spacer region and λ_0 is the free-space wavelength. Because the leakage amplitude is linear in $\Delta\phi$, the radiative linewidth scales as $\gamma_{\mathrm{rad}} \propto (\Delta\phi)^2$, or equivalently, $Q_{\mathrm{rad}} \propto (\Delta d)^{-2}$, until absorption, disorder, or finite-size leakage becomes dominant. In the large-d regime where the near-field coupling is weak, bilayer spectra can often be understood as interference between a Fabry–Pérot-like multilayer background and a resonant guided-mode channel, where the resonance spectrum becomes cleaner and more readily engineered (Fig. 2d).

The same interlayer coupling that produces suppressed leakage also makes the entire band structure reconfigurable. The dispersion of a bilayer PhC can be viewed as two sets of fundamental modes (a symmetric set and antisymmetric set), the frequency separation $\Delta f(d)$ between which is set by the interlayer coupling strength. When d is large and near-field coupling becomes weak, the two sets of modes are nearly degenerate. When d is small and near-field coupling becomes strong, the two sets of modes split and shift, which is also reflected in band splitting and band-edge shifts. (Fig. 2e) As a result, varying the interlayer gap can manipulate the position of BICs in $(\omega, \mathrm{k}_{\parallel})$-space; importantly, a SP-BIC remains pinned at Γ but frequency changes when d is small. In the large-d limit (weak coupling), the symmetric/antisymmetric modes become nearly degenerate, whereas an FP-BIC can move in momentum space as d is tuned [9].

Representative engineering applications of aligned bilayer physics include the double-layer Fano-resonance photonic-crystal filter, spatial light modulator, and enhancement of light-matter interaction.[16, 18, 22–24]. For example, one work uses the aligned bilayer to reshape the linewidth and line shape. In their optimized designs, a single-layer filter example reaches $Q \sim 4.5 \times 10^3$, whereas a double-layer design reaches $Q \sim 9.8 \times 10^4$. These results illustrate how the addition of one extra layer can suppress leakage without changing the symmetry [22]. (Fig. 2f).

Design takeaway: The aligned bilayer is the baseline configuration as it simply adds a vertical degree of freedom without relaxing in-plane momentum conservation. The in-plane lattice determines which collective Bloch resonances exist, while the interlayer spacing controls how those resonances behave as a coupled system: it tunes a real coupling (bonding/antibonding splitting and dispersion renormalization) and, independently, a radiative phase delay that sets interference in the shared continuum. This is why a second layer can deliver high-Q operation without changing lateral symmetry, but also why two high-Q routes have distinct robustness: SP-BICs inherit symmetry protection and tolerate d-variation, whereas FP-BICs are interference-quantized and therefore highly d-sensitive. The same two-mode and common radiation channels picture applies across photonic-crystal slabs, guided-resonance metasurfaces and plasmonic lattices, and provides a portable design grammar for bilayer filters, modulators and enhanced light–matter interaction platforms.

3 Bilayer lattices with lateral misalignment

In contrast to perfectly aligned bilayer lattices, laterally misaligned bilayer structures have a finite in-plane displacement t between two otherwise identical layers and introduce a qualitatively distinct regime of photonic coupling. (Fig. 3a) This sliding degree of freedom breaks a subset of in-plane and out-of-plane symmetries while preserving the lattice periodicity, which enables rich control over band dispersion, radiation channels, and non-Hermitian topology that is inaccessible in monolayer or aligned bilayer systems.

3.1 Modification of SP-BICs

For aligned bilayers, SP-BICs typically arise from incompatibility in symmetry between guided resonances and free-space radiation channels. Introducing an in-plane displacement t fundamentally alters this picture. Several works have shown that even an infinitesimal lateral displacement lifts the symmetry protection for the BIC at Γ-point, converting SP-BICs into high-Q quasi-BICs. As the lateral displacement increases, the Γ-point mode evolves continuously into split hybrid resonances with finite linewidth [9, 20, 25–28] (Fig. 3b).

From an interference perspective, the lateral displacement introduces a relative phase factor in the interlayer coupling and induces hybridization between otherwise degenerate guided resonances [25, 29–31]. Coupled bilayer structures also give rise to a dynamic and smooth

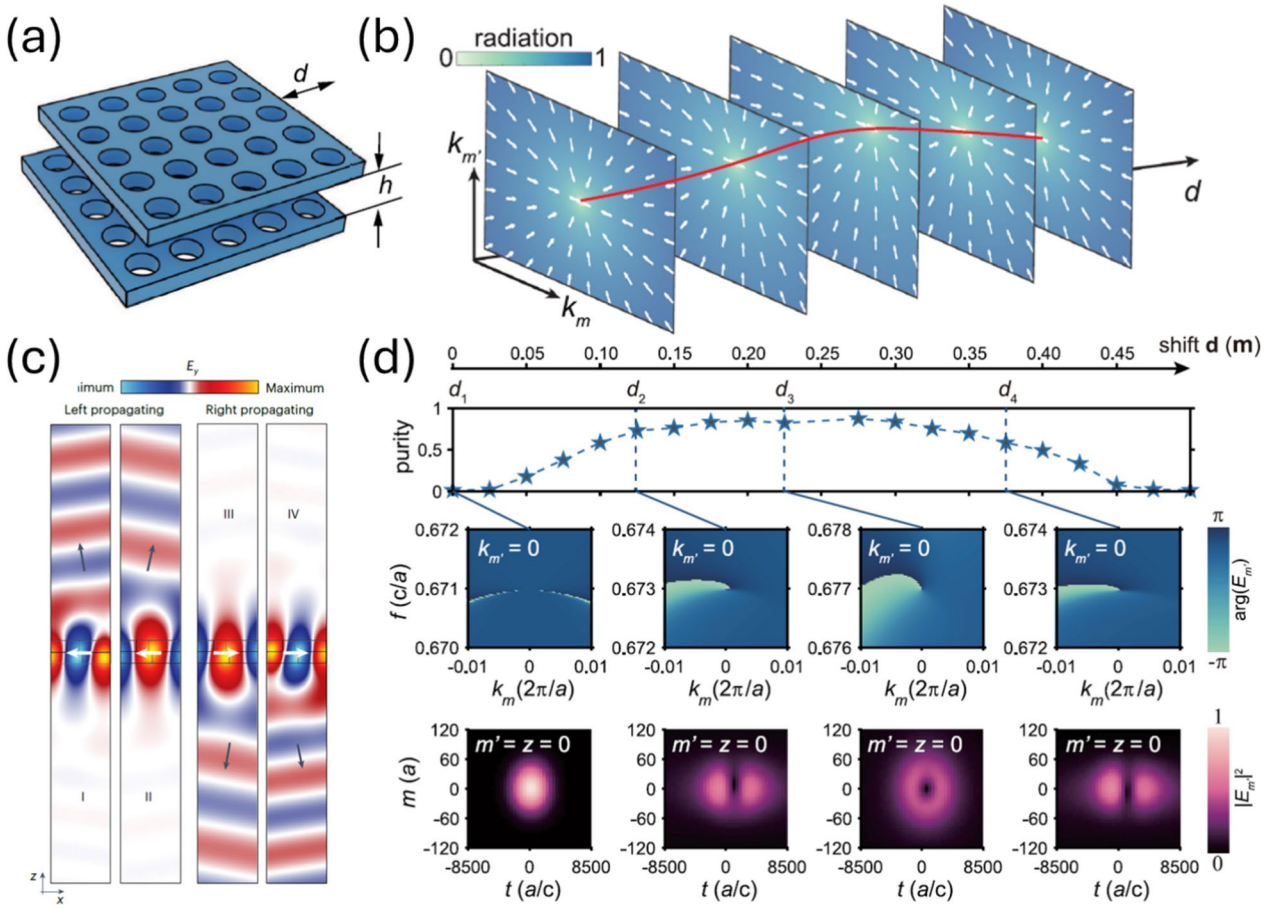


Fig. 3 Lateral displacement in bilayer photonic-crystal slabs enables reconfigurable radiation topology and spatiotemporal vortices. **a** Schematic of a bilayer photonic-crystal slab with an interlayer separation (denoted *h* in the schematic) and an in-plane sliding displacement between two otherwise identical lattices (denoted d) [9]. **b** Far-field polarization ellipses (white) overlaid on the radiated power in momentum space as t is varied, illustrating displacement-controlled redistribution of radiation channels and the migration of polarization singularities/BIC-derived leakage minima (trajectory indicated by the red curve) [9]. **c** Representative eigenmode profiles E_y for left- and right-propagating hybrid states. White arrows indicate the direction of guided-resonance energy flow, while black arrows indicate the dominant leakage-radiation direction, highlighting the emergence of displacement-controlled directionality (UGR-like behaviour) [32]. **d** Displacement-tunable spatiotemporal optical vortices: orbital-angular-momentum (OAM) purity versus sliding displacement (top), corresponding phase maps arg($E_{m'}$) in frequency–momentum space (middle; shown for a slice at $k_{m'} = 0$), and time-resolved transmitted-field intensity $|E_{m'}|^2$(bottom) for four representative displacements (t_1, t_2, t_3, t_4) along the *m* direction (values as indicated) [9]. Panel **a**, **b**, and **d** are reprinted with permission from Ref. [9]. Copyright 2024 by the American Physical Society. Panel **c** reprinted with permission from Ref. [32]. Copyright 2025, Springer Nature/SNCSC

crossover from SP-BICs to interference-based quasi-BICs through the lateral displacement. Importantly, these effects occur without breaking the overall lattice periodicity, while the quality factor remains highly tunable and robust over a broad parameter range.

3.2 Emergence of off-Γ BICs and unidirectional guided resonances

In bilayer lattices with broken up–down mirror symmetry, Γ-point BICs (usually SP-BICs) are generally fragile under lateral displacement. By contrast, off-Γ BICs (usually FP-BICs) often emerge and become the dominant organizing feature of the band topology. The radiation field of the off-Γ BICs is associated with polarization singularities. When the up-down mirror symmetry is broken, the radiation fields associated with off-Γ polarization singularities become asymmetric between the two half-spaces. Lateral displacement acts as a synthetic parameter controlling the relative phase between counter-propagating guided modes and the momentum of the polarization singularities. At critical displacement values, the coupling amplitude to one radiative channel, and therefore the corresponding partial radiative decay rate, vanishes. This produces forbidden emission into that half-space, while the opposite radiation channel can remain open. As a result, guided resonances can

radiate preferentially into one half-space while remaining dark in the opposite channel; these states are commonly referred to as unidirectional guided resonances (UGRs) [9, 11, 28, 32, 33] (Fig. 3c). This mechanism has been experimentally demonstrated in several works through the angle-resolved transmission and photoluminescence measurements. These results establish lateral displacement as a powerful route to engineer directional light–matter interactions without relying on external mirrors, absorbers, or geometric chirality [34].

Beyond lateral displacement, hetero-bilayer PhC slabs break up–down symmetry through material and thickness contrast while preserving lattice alignment. The resulting non-Hermitian interlayer hybridization, introduced in Sect. 2.3, produces UGRs organized around an interlayer BIC in a synthetic parameter space (e.g., set interlayer and intralayer propagation phases), yielding directionality that can persist across an extended wavevector [21].

3.3 Spatiotemporal and momentum–frequency singularities induced by translation

Beyond modifying momentum-space topology, lateral displacement also introduces an additional phase degree of freedom that enables both momentum and frequency reconfigurability, and therefore spatiotemporal optical singularities [9, 35, 36]. In aligned PhC slabs, polarization and phase singularities typically reside in momentum space and are associated with Γ- or off-Γ BICs. When a finite displacement t is introduced, the relative in-plane phase between the two layers effectively shifts these singularities along continuous nodal lines in momentum space (Fig. 3d). More importantly, breaking the up–down mirror symmetry lifts the degeneracy between upward and downward radiation channels, allowing singularities to migrate into $(\omega, \mathrm{k}_{\parallel})$ space. This migration manifests as spatiotemporal optical vortices carrying transverse orbital angular momentum (OAM) (Fig. 3d). Moreover, the position, charge, and purity of these spatiotemporal vortices can be continuously tuned by the sliding displacement and interlayer separation, providing a compact, on-chip route to multidimensional structured light.

3.4 Synthetic dimensions and non-Hermitian topology

The lateral displacement parameter t can also be interpreted as a synthetic momentum dimension that elevates one- or two-dimensional photonic lattices into higher-dimensional topological systems. Within this synthetic space, lateral displacement induces topological nodal phases, characterized by Dirac points, Fermi-arc-like edge states, or quantized complex Berry phases in non-Hermitian band structures [37, 38]. By tuning the sliding parameter, one can reconstruct Fermi arcs, switch between trivial and topological phases, and modulate radiation loss in a topologically protected manner [39]. This synthetic-dimension perspective also unifies BICs, UGRs, and asymmetric radiation as manifestations of underlying topological singularities in extended parameter space, rather than isolated resonant phenomena. Plasmonic multilayers provide another example of symmetry-controlled non-Hermitian topology. Spatial symmetry breaking can hybridize detuned plasmonic resonances through complex coupling, producing exceptional points where both resonance frequencies and linewidths coalesce and enabling nanoscale sensing [40].

Design takeaway: Lateral displacement t is best viewed as a continuous interference coordinate that rephases how the two layers couple to each other and to the same external radiation channels while preserving periodicity. This single geometric control therefore explains a broad set of results within one logic of radiation-topology control: Γ-point SP-BICs become tunable quasi-BICs, polarization singularities migrate in momentum space, and when up–down symmetry is broken, directionality emerges through asymmetric coupling to the two half-spaces. A useful generalization is to interpret t as a synthetic dimension, where BICs, UGRs, and spatiotemporal vortices correspond to different slices of a non-Hermitian band structure defined over (k, t, d), which is why the same actuation can tune Q, beam asymmetry and OAM in a unified way. From a device perspective, this makes laterally shiftable bilayers a particularly natural target for MEMS-enabled reconfigurable flat optics.

4 Moiré bilayer superlattices from lattice mismatch, stretch, or unequal unit cells

The bilayer flat optics discussed in the previous section have a relative lateral displacement between the layers, but without any difference in periodicity. In this section, we will discuss moiré bilayer flat optics, which possess a lattice mismatch between the layers. By keeping the two layers parallel but introducing a slight lateral incommensurability (for example, $a_1 \neq a_2$, uniaxial stretch, or unequal unit-cell sizes along x), the original single-layer periodicity is replaced by a long-period superlattice (or quasiperiodic modulation) (Fig. 4a). The resulting moiré envelope varies slowly across the device, creating locally distinct stacking registries and therefore spatially varying effective interlayer coupling. When the mismatch is commensurate, the structure admits a well-defined moiré supercell and a Bloch-band description in the reduced Brillouin zone [41].

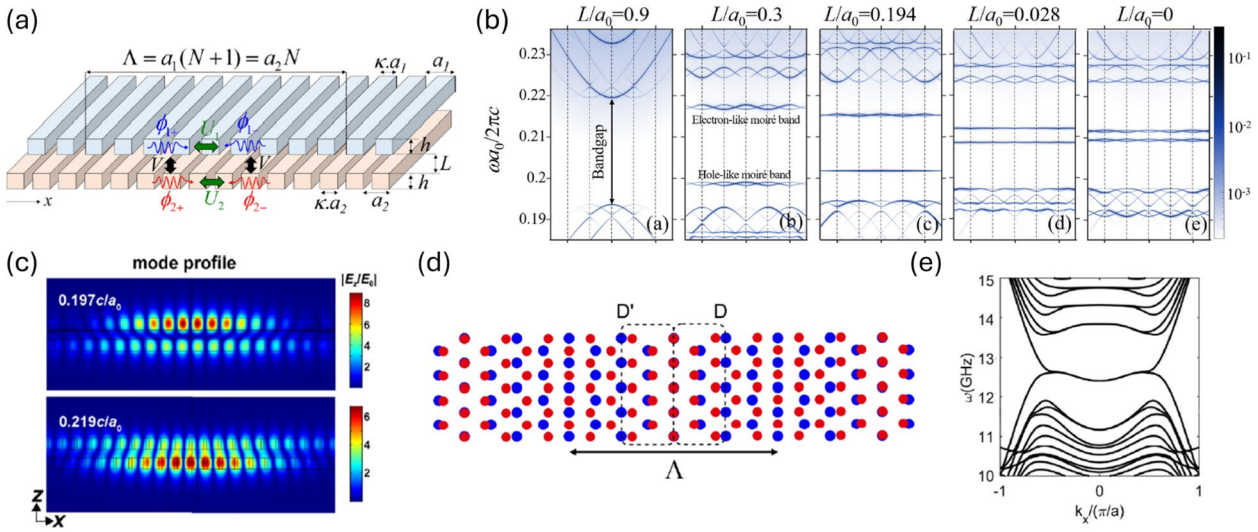


Fig. 4 Flatbands, moiré localization and synthetic gauge fields in laterally mismatched bilayer superlattices. **a** Commensurate 1D moiré bilayer formed by stacking two parallel gratings with slightly mismatched periods a_1 and a_2 ($a_1/a_2 = N/(N+1)$), producing a long supercell of length Λ. The interlayer separation d(denoted L in the schematic) controls the strength and phase of interlayer coupling [46]. **b** Calculated band structures for different interlayer separations, illustrating how coupling tunes the moiré minibands and can isolate nearly dispersionless bands inside a spectral gap (flatband formation as transport along the superlattice direction is suppressed) [46]. **c** Representative eigenmode profiles at two flatband frequencies, showing Bloch mode with an envelope localized on the moiré scale (momentum-free trapping), i.e., cavity-like confinement emerging from band folding and interlayer hybridization rather than an engineered point defect [41]. **d** Example of a lattice-constant-mismatched bilayer metacrystal generating a 1D moiré fringe pattern with quasiperiod Λ. The slowly varying local registry defines distinct effective magnetic-field domains (D and D') in the synthetic-field description [51]. **e** Corresponding effective-Hamiltonian band diagram showing Landau-level-like flat bands and associated dispersive domain/edge modes [51]. Panels **a**, **b** are reproduced from Ref. [46] under the terms of the Creative Commons Attribution 4.0 International License. Panel **c** is adapted from Ref. [41] under the terms of the Creative Commons Attribution 4.0 International License. Panels **d**, **e** are reprinted with permission from Ref. [51]. Copyright 2020 by the American Physical Society

4.1 Flat-band and localization

In laterally mismatched bilayers, a small mismatch between two nominally parallel lattices generates a long-period moiré supercell. This long-wavelength modulation folds guided-resonance dispersions into minibands. A typical outcome is multiple flattened dispersions and unconventional localization of optical fields within one moiré period, often accompanied by quasi-BIC-like radiation suppression and thus high-Q resonances [41–45]. Throughout this class of structures, the interlayer separation d remains a central control knob because it sets the strength and phase of interlayer coupling. (Fig. 4b).

The central consequence is not merely band folding, but also the emergence of a spatially modulated interlayer coupling within a single supercell. Different local stacking registries (such as mostly overlapped regions versus weakly overlapped regions) hybridize the two layers with different strengths. As a result, the extended Bloch-wave problem is converted into a miniband optical transport problem, in which propagation across the moiré lattice can be strongly suppressed in the superlattice direction [41, 46]. It is useful to distinguish lateral and temporal confinement. Weak intercell coupling narrows the moiré miniband and reduces the group velocity, so the optical envelope is localized on the moiré scale. A high Q, in contrast, indicates suppressed out-of-plane radiation and slow temporal decay. The two effects are complementary: flat-band localization confines the field spatially, while high Q allows the localized field to persist long enough to enhance the local density of states, Purcell factor, and nonlinear response.

This picture immediately explains why flat dispersion and spatial localization often appear together in moiré bilayers. When the effective intercell optical transport is weak, minibands become narrow, the group velocity is reduced, and optical modes preferentially localize within specific regions of each moiré period. (Fig. 4c) Because radiation leakage can be simultaneously suppressed by symmetry and interference inherited from the parent slabs, these localized states frequently acquire quasi-BIC-like character [41]. From this viewpoint, Bloch-like modes of the underlying lattice remain intact, but their envelope becomes trapped within the moiré supercell. In moiré bilayer flat optics, this has been described as momentum-free trapping of Bloch waves: the field retains

its Bloch character at the lattice scale, while localizing on the moiré scale. This mechanism enables simultaneous lateral confinement and suppressed vertical radiation, even when the mode lies above the light cone.

The moiré superlattice behaves as a distributed cavity array with reconfigurability in its location. Each moiré unit cell can host a localized electromagnetic mode whose spatial extent is set by the moiré period and whose field concentrates in the most strongly coupled stacking regions. Importantly, these moiré cavities are not defect cavities in the conventional sense. A useful benchmark is provided by conventional photonic-crystal defect cavities. For example, L3 nanocavities can reach measured unloaded Q values of 1.96×10^6 with $V \sim 0.96(\lambda/n)^3$, corresponding to $Q/V \sim 2 \times 10^6(\lambda/n)^{-3}$.[47] Other optimized photonic-crystal nanocavities, including heterostructure, nanobeam, and slot cavities, can further improve either Q, V, or Q/V, although often with different trade-offs in footprint, fabrication tolerance, emitter placement, and out-coupling. Reported simulation of twisted bilayer PhC has an effective Q/V on the order of 10^6–$10^7(\lambda/n)^{-3}$.[41] However, a direct experimental demonstration of this simultaneous high-Q, small-V regime, with both Q and V extracted in the same twisted bilayer PhC cavity, remains lacking. The same twisted bilayer PhC cavities are therefore best viewed as complementary to conventional defect cavities rather than universally superior in absolute Q/V: the confinement emerges from band folding combined with interlayer hybridization, which reshapes the dispersion into minibands and suppresses leakage channels through symmetry and interference inherited from the bilayer system. [41] Their distinctive value therefore lies in defect-free flatband localization, supercell-array scalability, spatially extended high density of states (DOS), improved tolerance to emitter position, and geometric tunability through mismatch, twist, and interlayer spacing.

Flat bands play a central amplifying role in this context. By guaranteeing a high-DOS and reduced group velocity, flat bands enhance field buildup and cavity effects. However, it is important to emphasize that visually cavity-like localization does not require a perfectly flat band. Local band-edge effects, stacking-dependent coupling landscapes, and interference-mediated radiation suppression can already produce localized modes. Flat-band formation should therefore be viewed as an amplifier of cavity enhancement through increased DOS and slow light and a strong candidate for nonlinear process enhancement [48].

4.2 Finite-size considerations

In practical devices, moiré superlattices are finite and should be viewed as leaky cavities rather than infinite crystals. Non-Hermitian modeling shows that a single moiré supercell typically provides only moderate confinement (with representative values $Q \sim 10^3$), whereas multiple coupled supercells can support quasi-BIC-like states with orders-of-magnitude higher Q. [49, 50] The key design message is that a flat miniband alone is not sufficient: the structure must also provide enough spatial extent for destructive interference and leakage suppression to fully develop.

4.3 Moiré-fringe gauge fields and Landau-level flat bands

In stretched moiré honeycomb systems, spatially varying misalignment induces an inhomogeneous gauge field for Dirac-like dispersions, producing photonic analogues of Landau levels, including flat bands, together with domain and edge states [51] (Fig. 4d, e). This provides a complementary perspective: lateral mismatch is not only a route to moiré cavities, but also a route to synthetic-field and topological photonics without time modulation or site-by-site control [46].

Design takeaway: Lattice mismatch replaces a uniform interlayer coupling with a slowly varying coupling landscape within each moiré period, so the relevant design object becomes a moiré miniband whose envelope lives on the supercell scale. Flatbands and localization are therefore two sides of the same transport suppression: folding brings many branches into near resonance, while the modulated hybridization suppresses effective intercell tunnelling and concentrates energy in preferred stacking registries. This viewpoint unifies cavity-like moiré localization, quasi-BIC-like radiation minima and synthetic-field physics such as Landau-level-like flatbands, as different limits of the same ingredients: band folding, position-dependent hybridization and interference-mediated leakage suppression. The practical trade-off is footprint versus performance: ultra-high-Q states typically require several moiré periods for destructive-interference and leakage suppression to fully develop. Therefore, finite-size (non-Hermitian) cavity modelling should accompany miniband arguments when targeting device-scale implementations.

5 Twisted bilayer flat optics

Twisted bilayer flat-optics platforms, like the moiré bilayer superlattices discussed in the previous section, also form moiré superlattices, but the misalignment occurs in both in-plane directions. The interlayer twist angle θ, as a degree of freedom, converts a strictly momentum-conserving, single-lattice scattering problem

into a more complex momentum-mixing problem governed by two rotated reciprocal lattices. (Fig. 5a).

5.1 Moiré scattering and twist-angle dependent resonance

A foundational step is to formulate twisted bilayer PhC slabs directly as a multichannel scattering problem that does not rely on large commensurate supercells (whose size and computational cost blow up at small angles). Except for special commensurate angles, the twisted bilayer flat optics are generally quasiperiodic, so conventional periodic-boundary flat-optics tools cannot be applied straightforwardly [12, 41]. Instead, a high-dimensional plane-wave expansion is often used to explore the twist-dependent transmission, reflection, chiral response, and resonant field distributions. [52–54]

The key point is to define a channel basis. The first layer of flat optics scatters an incident plane wave with in-plane momentum $\mathrm{k_{inc}}$ to outgoing channels $\mathrm{k_{inc}} + \mathrm{g}^{(1)}$, described by a layer scattering matrix $\widetilde{S}^{(1)}(\mathrm{k_{inc}})$. In a bilayer, the second layer acts on this expanded set of channels, so the combined scattering naturally contains mixed indices $\mathrm{g}^{(1)} + \mathrm{g}^{(2)}$, i.e., moiré-enabled momentum conversion. (Fig. 5a) This is the reciprocal-space origin of twist-tunable spectral features: changing the twist angle θ changes which channel combinations fall near guided-mode dispersions, and which can couple efficiently to radiation. [52]

Twist does not merely perturb a resonance, it redefines the set of reciprocal vectors that mediate phase matching, thereby moving entire families of folded resonances in frequency–momentum space. Therefore, using the plane-wave expansion approach and the band-folding picture, one can also identify guided resonances whose frequencies are strongly twist-dependent (depend on the moiré wavevector) and those frequencies are twist-independent (associated with non-moiré vectors or different folding pathways) [52–59]. A visual validation of the moiré scattering picture comes from mapping the momentum-resolved band structure and isofrequency contours of twisted bilayer PhC slabs, where the isofrequency contours repeat under translations by first-order moiré reciprocal vectors, while higher-order repetitions are much weaker. (Fig. 5b) Moreover, the repeated contours are not perfectly identical, which is consistent with the incommensurate and quasiperiodic nature of generic twisted moiré lattices rather than strict crystallographic periodicity [53].

5.2 Polarization, chirality and spin–orbit conversion

Because of the moiré scattering effect, the twisted bilayer behaves as a coupled resonator stack whose eigenmodes acquire twist-dependent polarization states. By tuning twist angle and interlayer gap, one can continuously control the output Stokes vector, including polarization ellipse orientation and ellipticity. This type of multimode polarization manipulation has no direct analogue in single-layer PhCs and highlights that bilayer coupling enables polarization degrees of freedom inaccessible in planar designs [58, 60, 61]. For the same reason, a twisted bilayer can become intrinsically chiral even when each individual layer is planar and achiral. [60, 62–67]

Beyond static polarization conversion, twisted bilayers also provide a natural platform for spin–orbit photonics, where spin angular momentum (SAM) and orbital angular momentum (OAM) can be interconverted through twist-enabled momentum channels.[68] Because twist reshapes momentum-conversion pathways, opposite circular polarizations experience different moiré diffraction channels. As a result, light with zero net angular momentum can acquire different spin-orbital conversion in reflection and transmission, with the two effects exhibiting distinct dependencies on the interlayer separation d. This behavior does not rely on absorption or intrinsic

(See figure on next page.)

Fig. 5 Twisted bilayer flat optics: moiré scattering, radiative-channel engineering and twist-programmable dispersion. **a** Schematic of a twisted bilayer photonic-crystal slab (square lattice of holes) under normal incidence. Twisting rotates the two reciprocal lattices relative to each other, generating first-order moiré wavevectors that define the dominant momentum-conversion channels [52]. **b** Twist-enabled multichannel band folding and resonance imaging. Left: effective (Hamiltonian) band structure of a twisted bilayer slab (example: $\theta = 10°$), showing TE-like and TM-like branches and their coupling strengths. Right: measured isofrequency contours at selected frequencies, demonstrating that the observed resonance families repeat under translations by first-order moiré reciprocal vectors (higher-order repetitions are weaker), consistent with moiré scattering and quasiperiodic momentum mixing [53]. **c** Helicity-dependent moiré diffraction and spin–orbit conversion. A twisted bilayer can imprint spin and orbital angular momentum through polarization-dependent momentum transfer; diffracted orders can carry coupled SAM–OAM content set by the moiré reciprocal vectors [68]. **d** Twist-enabled radiative channeling from BICs. Moiré momentum mixing allows an at-Γ BIC in one layer to transfer energy to guided resonances in the other layer that couple to free space, opening a controllable leakage pathway (quasi-BIC formation) and enabling vortex emission when the radiative channel inherits a phase singularity [70]. **e** Time evolution of optical mode in twisted bilayer flat optics. Normalized amplitude and phase distributions of the LCP portion of the emission at different times after excitation. Panel **a** is reprinted with permission from Ref. [52]. Copyright 2021 by the American Physical Society. Panel **b** is reproduced from Ref. [53], AAAS. Panel **c** is reprinted with permission from Ref. [68]. Copyright 2025 by the American Physical Society. Panels **d**, **e** are adapted from Ref. [70] under the terms of the Creative Commons Attribution 4.0 International License.

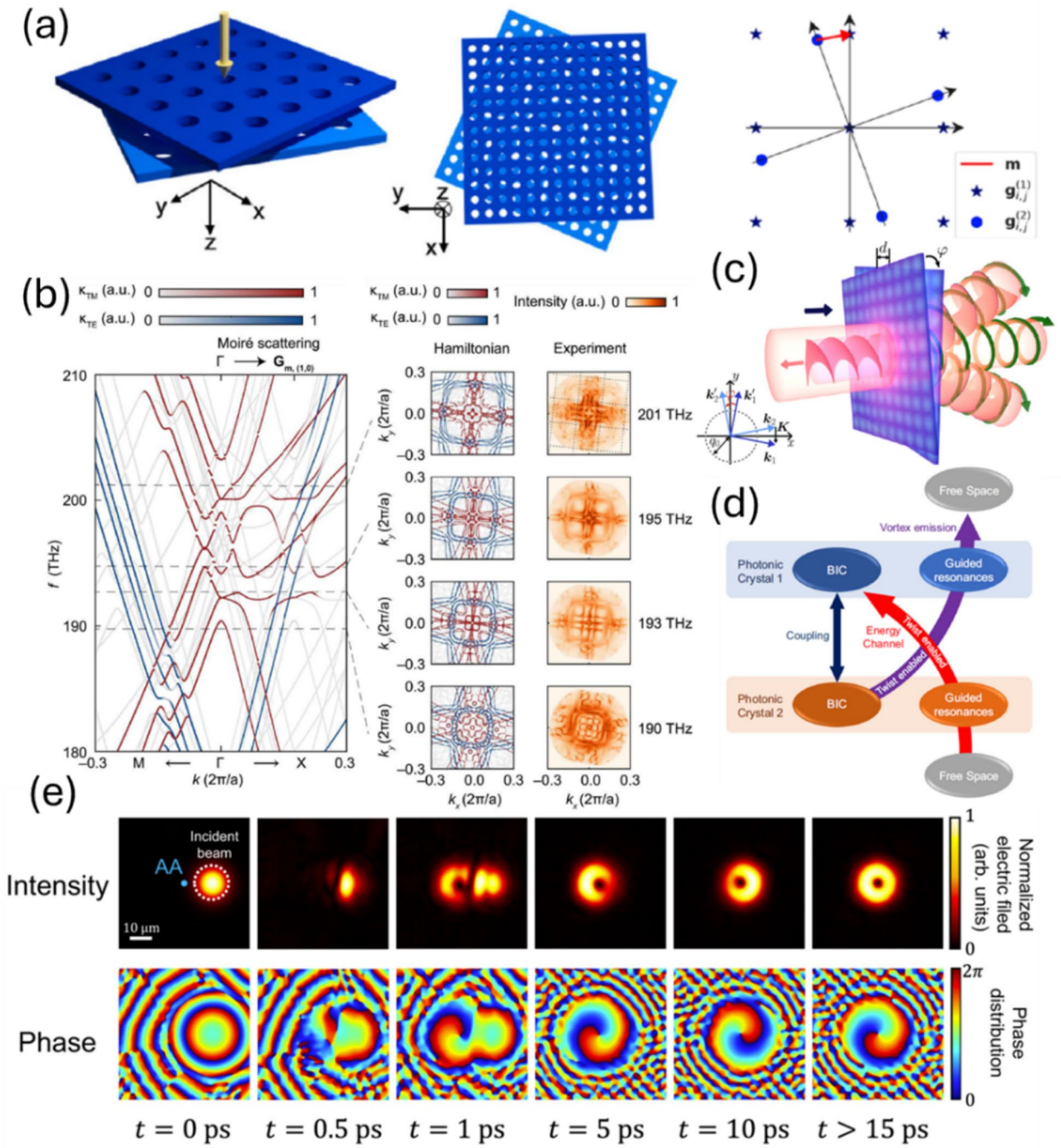


Fig. 5 (See legend on previous page.)

material chirality, instead, it arises from helicity-dependent interference between twist-enabled momentum channels.

When emitters or gain media are incorporated into the bilayer stack, the same physics governs chiral emission and lasing. Twisted bilayer flat optics can support orbital chiral lasing, where the handedness of the emitted OAM mode is selected by the interlayer coupling [69] (Fig. 5c). In both cases, chirality is not an add-on but an intrinsic property of the coupled bilayer system.

5.3 From tunable resonances to tunable leakage

The same moiré scattering mechanism that tunes resonance positions also reshapes radiative channels.

(Fig. 5d, e) As we introduced in previous sections, in a perfectly aligned bilayer the Γ-point SP-BIC remains decoupled, but a non-zero twist generates a moiré structure that breaks the strict short-range periodicity. Consequently, a BIC in one slab can couple to guided resonances in the other slab that are coupled to free space, enabling energy transfer between the BIC and radiation [70], and thereby forming a quasi-BIC [71]. Moreover, by decreasing twist angle, the quasi-BIC gradually approaches a perfect BIC with total radiation loss from all diffraction channels strongly suppressed. This radiative-channel interpretation is particularly aligned with the moiré scattering perspective: twist generates an enlarged moiré unit cell and when this moiré scale becomes large, higher-order diffraction channels beyond the zero order appear [71].

This coupling mechanism from BIC to quasi-BIC also generates radiation that carries optical vortices with topological charges [70] (Fig. 6a). Once the radiative pathway is opened by twist-enabled momentum mixing, moiré scattering becomes a way to synthesize far-field phase structure. These radiative pathways have therefore been termed "moiré channels". This idea has been realized as an orbital chiral lasing using bilayer twisted flat optics [69] (Fig. 6b). A recent study further reported a family of twist-induced quasi-BICs whose reciprocal-space distributions resemble truncated Bessel functions and whose real-space phase vortices are centered near AA-stacking regions. These modes have been experimentally identified as densely distributed resonant peaks that depend sensitively on the twist angle θ and the interlayer separation d. The moiré scattering degrees of freedom enable switching of the topological charge at a fixed wavelength by adjusting these geometric parameters: different resonant peaks can be shifted into the same operating wavelength so that optical vortices with different charges are selectively excited [72]. More precisely, these Bessel-type quasi-BICs should be understood as approximate analytical eigen-solutions of a continuum coupled-mode description near the Γ-point. In this limit, twist-induced moiré coupling mixes a quasi-continuum of guided resonances with different in-plane wavevectors. When the single-layer dispersion and the interlayer coupling kernel are expanded near Γ, the resulting momentum-space

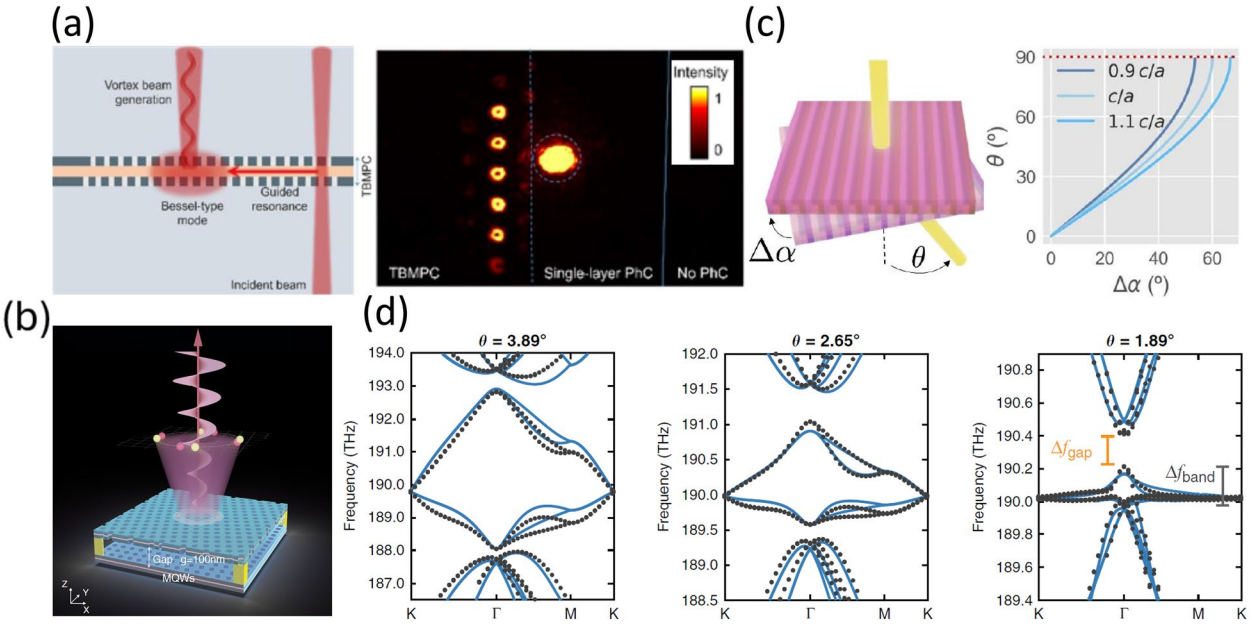


Fig. 6 **a** Vortex-beam generation from twisted bilayer moiré PhCs. Nonlocal excitation of Bessel-type guided-resonance channels produces far-field vortex arrays; representative measured intensity maps illustrate vortex emission confined to the moiré region and absent in single-layer references [72]. **b** Coherent vortex emission (orbital chiral lasing) enabled by twisted bilayer coupling, where gain and optical pumping select a chiral OAM-carrying mode supported by the bilayer radiation topology [69]. **c** Moiré scattering–based momentum engineering for beam steering. Two rotatable slabs with a relative in-plane rotation $\Delta\alpha$ provide a continuous knob for selecting a dominant diffraction order; the output polar angle θ follows a twist-dependent mapping that varies with frequency [76]. **d** Twist-induced moiré flatbands in hexagonal/honeycomb bilayers. Full-wave band structures (symbols) and continuum-model fits (lines) for decreasing θ show hybridization of displaced Dirac dispersions, opening a mini-gap Δ_{gap} and compressing the miniband bandwidth Δ_{band} toward a magic-angle-like flatband regime [12]. Panel **a** is adapted from Ref. [72] under the terms of the Creative Commons Attribution 4.0 International License. Panel **b** is adapted from Ref. [69] under the terms of the Creative Commons Attribution 4.0 International License. Panel **c** is adapted with permission from Ref. [76]. Copyright 2024 American Chemical Society. Panel **d** is adapted from Ref. [12] under the terms of the Creative Commons Attribution 4.0 International License

integral equation becomes approximately radially symmetric. This approximate radial symmetry leads to Bessel-function envelopes of the form $J_\ell(\alpha k)e^{i\ell\phi_k}$, where the integer ℓ gives the azimuthal phase winding and therefore the vortex or OAM order. Because the small-k continuum approximation breaks down at larger wavevectors and because the moiré Brillouin zone provides a finite momentum cutoff, the eigenmodes are truncated Bessel-type modes rather than infinite Bessel functions. Although first reported in photonic platforms, their emergence may suggest potential analogous mode formation in twisted systems beyond optics.

5.4 Moiré-scattering–enabled momentum engineering: beam steering and beamforming

From the moiré-scattering viewpoint, beam steering and beamforming in twisted bilayers are direct consequences of programmable in-plane momentum transfer. As the twist angle changes, the set of accessible in-plane momenta moves in k-space, and a subset of diffraction orders can fall inside the light cone (hence becomes radiative) and the corresponding emission angles become twist-tunable [73–75]. By carefully designing flat optics, one can route most power into a single selected order while canceling competing orders. For a selected twist-sensitive diffraction order, the polar angle depends primarily on the relative twist angle θ, whereas the azimuthal angle is controlled by the global rotation of the two slabs [76, 77]. (Fig. 6c) Plasmonic lattices also provide a related experimental implementation of twist-controlled radiative momentum selection. In stacked moiré plasmonic lattices, the relevant collective modes are surface-lattice resonances rather than guided resonances of dielectric PhC slabs. Dark surface-lattice resonances can mediate far-field interlattice coupling in the vertical direction, enabling twist-angle-controlled directional lasing even when the two nanoparticle lattices are separated far beyond the near-field coupling range [78]. This example shows that the same bilayer design logic applies: the interlayer geometry selects the allowed radiative momentum channels, although the performance trade-off is then governed by radiative coupling, gain, and Ohmic loss rather than purely by BIC-like leakage suppression.

5.5 Twist-induced moiré flat bands in bilayer flat-optics

One representative phenomenon of twisted bilayer flat-optics is the emergence of moiré minibands with strongly reduced bandwidth, often accompanied by field localization and high-Q-factor. This behavior has been reported across a wide range of systems including two-dimensional photonic-crystal slabs [12, 41, 79, 80], one-dimensional gratings [66], and plasmonic bilayers [81]. The underlying physics can be understood within a single, unified framework: moiré band folding and interlayer hybridization.

Twisting two identical periodic layers generates a long-wavelength modulation in real space and, correspondingly, a reduced moiré Brillouin zone in the 2D momentum space. As a result, multiple replicas of monolayer dispersion are folded into a small momentum region and brought into near resonance. Strong interlayer coupling then hybridizes these folded branches and converts band crossings into avoided crossings and reshapes the dispersion into minibands. When the hybridization scale becomes comparable to the twist-controlled kinetic scale, the miniband dispersion is strongly renormalized, which leads to narrow bandwidths and suppressed group velocity.

This competition can be expressed intuitively as a two-scale problem. The twist angle θ sets the moiré momentum scale k_θ, which determines how closely folded bands approach one another in momentum space, while the interlayer coupling strength Δ_b sets how efficiently these bands hybridize once they are brought together. Flat bands emerge when hybridization competes with the kinetic dispersion imposed by the twist, such that the miniband curvature collapses and transport across the moiré lattice is suppressed [12] (Fig. 6d).

Hexagonal and honeycomb photonic lattices provide a particularly transparent illustration of this mechanism. In these systems, the low-energy band structure near the Brillouin-zone center is well described by Dirac-like dispersions. Twisting displaces the Dirac cones of the two layers by a momentum offset k_θ; finite interlayer coupling then mixes the cones and opens avoided crossings. As the twist angle decreases, k_θ shrinks, so the same coupling strength becomes increasingly effective. In the regime where the hybridization scale competes with the Dirac kinetic term, the band velocity is strongly reduced and flat bands appear. Unlike electronic moiré materials, photonic platforms offer a crucial advantage: the interlayer coupling strength is not fixed, but can be engineered and tuned, most directly through the interlayer separation d, as well as through slab thickness, refractive-index contrast, and modal overlap [12].

The band-structure picture has a direct and intuitive real-space consequence. Once minibands become narrow, propagation across the moiré lattice is inhibited and optical modes localize within individual moiré supercells. Localization is typically strongest near mostly overlapped (AA-stacked) regions, where interlayer overlap and hybridization are maximal. In PhC slabs, this behavior has been described as momentum-free trapping of Bloch waves: the electromagnetic field retains the Bloch character of the underlying lattice at short length scales, while its envelope localizes on the

moiré length scale. This mechanism enables cavity-like confinement without introducing explicit defects and can simultaneously suppress vertical radiation through symmetry and interference inherited from the parent slabs, giving rise to quasi-BIC-like high-Q resonances even for modes above the light cone [12, 41].

In twisted bilayer flat optics, flat bands do not require extremely small twist angles if the system is engineered into a sufficiently strong-coupling regime. In strongly coupled twisted bilayer flat optics, flat bands can appear at large twist angles and persist over broad angular ranges. In these cases, stronger interlayer coupling activates higher-order momentum mixing in an extended Brillouin-zone picture and generates additional avoided crossings that flatten the dispersion and localize fields. [66]

5.6 Topological transitions in twisted bilayers

Beyond polarization optics, twisting can serve as a geometric control parameter for topological states and their scattering in bilayer platforms. For example, Fermi-arc (a topological surface state) reconstruction was observed in twisted photonic Weyl meta-crystals. While each block individually preserves lateral symmetry, twisting induces aperiodic hybridization and scattering of Fermi arcs at the interface [82]. Another work reported that twisting a bilayer magnetic hyperbolic metasurface enables topological transition of the iso-frequency contour from a closed ellipse to an open hyperbola [83].

5.7 Special case: merged or in-plane moiré photonic crystals at $d = 0$

A closely related limit is the merged or in-plane moiré photonic crystal, where two lattices are patterned in the same slab rather than separated by a vertical spacer. This geometry can be viewed as an adjacent $d = 0$ platform in the broader (d, θ) design space, although the coupling is mediated by in-plane index modulation rather than by an interlayer gap. Such merged structures share many core moiré mechanisms with vertically stacked bilayers, including twist-controlled miniband formation, flat-band localization, and inter-lattice coupling. They have enabled magic-angle nanolasers [84–88], phase-synchronized moiré nanolaser arrays [89], ultra-high-Q twisted-lattice nanocavities [90, 91], enhanced nonlinearity [48, 92, 93], and cavity quantum electrodynamics [94, 95]. Compared with vertically separated bilayers, merged moiré lattices are generally easier to fabricate and align because they avoid transfer, spacer control, and layer-to-layer registration. However, this simplicity comes at the cost of reduced post-fabrication reconfigurability: the interlayer gap, relative translation, and twist angle are fixed once the pattern is written.

Design takeaway: Twist is qualitatively distinct from sliding and mismatch because it rotates the entire reciprocal lattice: it does not merely shift a resonance but redefines the momentum-transfer channels available to the stack. Consequently, θ tunes three outcomes at once: (i) resonance positions in (ω, k) via moiré folding, (ii) radiative leakage by twist-enabled channels (quasi-BIC engineering), and (iii) polarization and phase configuration in the far field through multi-channel interference (chirality, SAM–OAM conversion, vortex emission and beam steering). Across dielectric, plasmonic and grating platforms, a compact organizing principle is a two-parameter competition: θ primarily sets the moiré kinetic scale (how close folded dispersions are brought in momentum space), whereas d primarily sets the interlayer hybridization scale. Many seemingly diverse observations such as twist-tunable resonances, moiré quasi-BICs, beam steering, and both small-angle and large-angle flatbands, can be interpreted as different operating points in this (θ, d) map. This suggests a practical workflow: choose the desired regime (few vs many radiative channels; weak vs strong coupling), then use θ and d as largely orthogonal knobs to target spectral tunability, leakage control and far-field structuring without redesigning the in-plane lattice.

6 Bilayer flat optics with locally twisted meta-atoms

In bilayer flat optics with locally twisted meta-atoms, the two layers share the same in-plane lattice vectors, but the meta-atom orientation in the upper layer is rotated relative to that in the lower layer. The structure therefore remains periodic in the transverse plane (no moiré supercell and no band-folding in the lattice sense) yet becomes three-dimensionally chiral, because the bilayer breaks the mirror symmetry with respect to the flat optics plane. This configuration is conceptually distinct from global twist platforms, as its physics is dominated by interlayer coupling inside a unit cell, rather than by momentum mixing across many reciprocal-lattice replicas.

6.1 Chirality from a coupled-meta-atom viewpoint

Locally twisted meta-atoms are usually viewed as vertically coupled oscillators. Two resonant elements (e.g., plasmonic rods) are arranged such that their dominant dipole moments are non-parallel and are separated along the propagation direction. The near-field coupling between two relatively rotated meta-atoms often yields a pair of eigenmodes whose optical responses produce strong polarization dependence[96] and circular

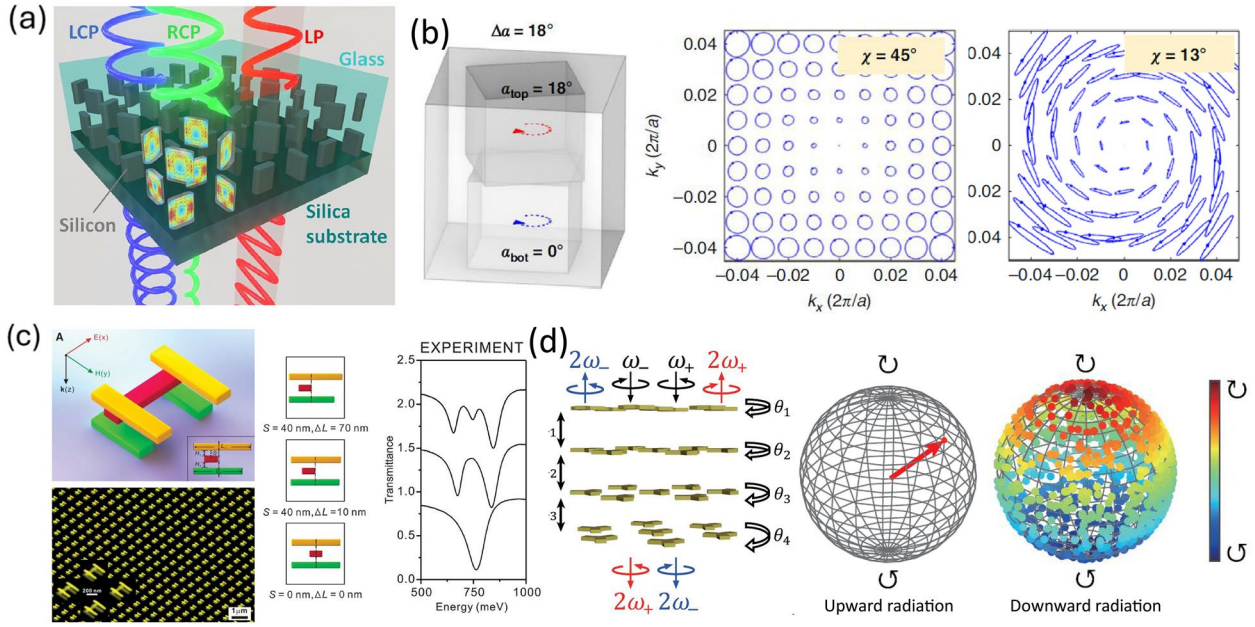


Fig. 7 Locally twisted bilayer flat optics and multilayer flat optics: cascaded coupling. **a** Locally twisted bilayer dielectric metasurface supporting a chiral supermode arising from strong vertical coupling between stacked planar resonators. Although each layer is individually achiral, interlayer hybridization produces a collective three-dimensional chiral response with large optical activity [103]. **b** Locally twisted bilayer dielectric metasurface. A structure with identical relative twist $\Delta\alpha = 18°$ but different absolute orientations of the top and bottom layers ($\alpha_{top} \neq \alpha_{bot}$). The corresponding far-field polarization maps show circularly polarized emission near a BIC in the upward direction, while the downward radiation exhibits a different ellipticity [110]. **c** Example of a three-layer plasmonic metasurface formed by vertically stacked meta-atoms with different orientations. Relative displacements and separations between layers tune near-field hybridization, providing strong sensitivity of the optical spectrum to three-dimensional geometry and illustrating cooperative vertical coupling in multilayer metamaterials [112]. **d** Cascaded bianisotropy and nonlinear control in multilayer metasurfaces. Stacking multiple nonlinear flat-optics layers with independently tunable interlayer spacings d_j and twist angles θ_j enables arbitrary control of interference and polarization at both the fundamental and harmonic frequencies. As a result, the effective nonlinear susceptibility tensor can be engineered to span the full Poincaré sphere, supporting programmable polarization, chirality, and directionality of the emitted nonlinear light, including unidirectional second-harmonic generation [60]. Panel **a** is adapted with permission from Ref. [103]. Copyright 2020 American Chemical Society. Panel **b** is adapted from Ref. [110] under the terms of the Creative Commons Attribution 4.0 International License. Panel **c** is modified from Ref. [112], AAAS. Panel **d** is reprinted with permission from Ref. [60]. Copyright 2025 by the American Physical Society

dichroism [97–102]. The chirality is governed by interlayer coupling strength and phase delay and is therefore controlled by the interlayer distance d and the twist angle θ.[98, 101] (Fig. 7a) With additional geometric degrees of freedom in the meta-atom design, chirality can also arise from different interlayer electromagnetic interactions, including electric–electric, magnetic–magnetic, and magnetoelectric channels, and, in some regimes, higher-order multipoles.[96, 103, 104] Given these properties, locally-twisted flat optics has become a practical strategy for chiral sensing [105].

6.2 BICs and arbitrary polarization control

Locally twisted flat optics become particularly powerful when combined with BICs and quasi-BICs, providing a route to simultaneously engineer high-Q resonances, polarization selectivity, and chirality. By engineering interference and polarization using the interlayer distance d and twist angle θ, one can obtain a quasi-BIC mode together with the circular polarization channel. [103, 106–109] With further meta-atom design, this concept can be extended to BICs supporting arbitrary polarization states spanning the entire Poincaré sphere [110] (Fig. 7b).

Design takeaway: Local twist provides a meta-atom route to chirality and polarization selectivity without invoking moiré supercells: the lattice remains strictly periodic, but the unit cell becomes a genuinely three-dimensional chiral object whose eigenmodes are set by interlayer coupling. This is why coupled-oscillator/Born–Kuhn-type models generalize well across plasmonic and dielectric implementations: relative orientation defines the allowed bianisotropic pathways, while the spacing d controls their strength and phase, setting optical activity and circular dichroism without

re-patterning. Crucially, when combined with BIC or quasi-BIC design, local twist can decouple polarization/chirality selectivity from linewidth control, enabling high-Q chiral resonances and access to arbitrary polarization states on the Poincaré sphere. From an implementation viewpoint, this configuration is attractive when one wants strong chiroptics with compact unit cells and without the fabrication/simulation burden of very large moiré superlattices.

7 Towards more complexity and more functionality: multilayer flat optics

The above discussion about bilayer flat optics highlights a central message: once two patterned layers are brought into a shared electromagnetic environment, the *interlayer degrees of freedom* (such as spacing d, translation t, and relative twist angle θ) become the major design parameters that can substantially reshape mode hybridization, radiative interference, and far-field channels. Multilayer stacks generalize this idea from a two-mode problem to a coupled-layer network, where several degrees of freedom d_j, t_j, and θ_j, and therefore multiple coupling pathways coexist. Even without introducing any new in-plane pattern complexity, adding a third (or N-th) layer provides qualitatively new capabilities: (i) engineered spectral bandwidth and effective medium response through cooperative vertical coupling; (ii) cascaded polarization and chirality control through sequentially twisted anisotropic sheets; (iii) nonlinear phase matching and multidimensional tuning via layer-by-layer phase engineering; (iv) BIC-derived singular fields and optomechanical forces with additional reconfigurability; and (v) higher-order flatband engineering by coupling flatbands to flatbands rather than only flattening dispersive bands.

7.1 Stronger coupling in multilayer stack

One of the motivations for multilayer flat-optics is to translate flat-optics concepts into bulk-like 3D metamaterials without abandoning planar nanofabrication. In these three-dimensional metamaterials, the optical response of the stacked layers is governed by interactions between adjacent layers and evolves systematically with the number of layers [111]. As the number of layers increases, the spectra evolve in a manner consistent with cooperative vertical coupling: resonances become stronger and broader due to increased oscillator strength and enhanced collective interaction, while new bands emerge as energy splitting develops from strong interlayer coupling between neighboring layers. The multilayer coupling can also be engineered to generate sharp spectral features by exploiting interactions between modes with different symmetry [112]. (Fig. 7c) As a result, the optical response is highly sensitive to 3D structural changes because, in the near-field regime, the relevant hybridization can be more distance-dependent than conventional dipole–dipole coupling.

7.2 Cascaded bianisotropy

Multilayer stacks are also a natural setting for cascaded bianisotropy. As discussed above, in a bilayer flat optics, twist turns two achiral sheets into a chiral system. In a multilayer stack, sequential twist creates a distributed chiral coupling pathway that can broaden and stabilize polarization selectivity. [113]

Cascaded bianisotropy is especially impactful for nonlinear optics, where each layer, as an individual nonlinear source, provides a discrete and engineerable phase delay. By stacking aligned nonlinear flat-optics on top of each other and tune the interlayer distances d_j, one can achieve phase matching in the unconventional backward direction and linear scaling of second harmonic generation intensity with the number of layers. [114] Going one step further, introducing twist angles θ_j between successive layers as additional degrees of freedom enables full control of interference and polarization in both the forward and backward directions. In this sense, multilayer flat-optics platforms can be viewed as effective media, in which the effective nonlinear susceptibility tensor can be arbitrarily tailored. As a result, the emitted nonlinear light can exhibit programmable polarization, chirality, and directionality, including fully controllable unidirectional emission [60] (Fig. 7d).

7.3 Complex band transition and flatband in multilayers

One study reported that by modulating the interlayer spacings d_j, and hence the coupling strengths, multilayer flat-optics systems can undergo band transitions, enabling systematic engineering of the optical singularities associated with the transformed bands. This behavior can be viewed as a multilayer extension of bilayer BIC physics: once a third layer is introduced, both the number of accessible singularities and the degrees of freedom available to displace them increase substantially [115].

A complementary approach constructs triple-layer superlattices by stacking two double-layer superlattices that already host fundamental moiré flat bands. Importantly, flatband–flatband coupling does not generically guarantee another flat band; interband coupling can also introduce dispersion if the coupling strength or detuning varies strongly with momentum. Hybrid moiré flat bands are obtained only under suitable conditions, such as small parent-band bandwidths, appropriate spectral detuning, strong spatial overlap between the parent modes, and

sufficiently uniform or engineered coupling across the relevant momentum range. Under these conditions, recent theoretical analysis and full-wave simulations show that coupled fundamental moiré flat bands can form hybrid moiré flat bands, with controllable spatial mode profiles and, in some cases, improved flatness compared with the parent bands [116].

Design takeaway: Multilayer stacks extend bilayer flat optics from a two-mode interference picture to a coupled-network picture: each added layer introduces new supermodes, additional radiative pathways and extra phase delays, allowing spectral shaping, chirality and nonlinear emission to be distributed across the stack rather than demanding an extreme response from a single sheet. A useful generalization is to view an N-layer platform as a vertical coupled-resonator chain whose coupling matrix is programmed by $\{d_j, t_j, \theta_j\}$, naturally explaining cooperative evolution of oscillator strength, mode splitting and emergent bands with layer number and motivating effective-medium descriptions when the overall thickness remains subwavelength. In terms of what becomes achievable, multilayers enable capabilities that are difficult in bilayers, such as multilayer-controlled nonlinear phase matching, richer BIC-derived singularity landscapes, and hybrid moiré flat bands formed through engineered flatband–flatband coupling under suitable detuning and mode-overlap conditions, at the cost of increased fabrication and alignment complexity.

8 Conclusion and outlook

In this Review, we have surveyed recent progress in coupled bilayer and multilayer flat optics as platforms for reconfigurable control of light. By introducing interlayer degrees of freedom, such as spacing, lateral translation, and relative twist, bilayer and multilayer flat optics acquire qualitatively new capabilities that are inaccessible in monolayer architectures. Across diverse material platforms and dimensionalities, these additional degrees of freedom reshape mode hybridization, radiation channels, and band topology, enabling phenomena including tunable resonance, optical singularities, moiré-induced flat bands and localization, programmable chirality and spin–orbit conversion, directional and vortex emission, and enhanced linear and nonlinear optical responses. Bilayer and multilayer flat optics should be viewed not as minor extensions of planar metasurfaces, but as coupled-layer networks, where interference, symmetry, and hybridization can be engineered in a high-dimensional parameter space. This perspective provides a coherent physical framework that connects band folding, non-Hermitian radiation physics, and effective-medium behavior across seemingly disparate implementations.

Looking ahead, the impact of bilayer and multilayer flat optics will increasingly depend on advances that move beyond proof-of-principle demonstrations toward scalable, dynamically reconfigurable, and system-level platforms. Progress in advanced nanofabrication and heterogeneous integration, including high-precision alignment and flip and stacking techniques[53, 63, 69, 73, 107, 117, 118] will be essential for realizing complex multilayer architectures with reproducible performance. At the same time, the incorporation of reconfigurable photonics techniques, such as micro- and nano-electromechanical systems (MEMS/NEMS)[58, 119] techniques and DNA origami techniques[120] offers a particularly promising route to in situ and high-speed control of interlayer spacing, twist, and translation, enabling real-time reconfigurability of the functionalities discussed above.

At the same time, dynamic mechanical reconfiguration introduces stringent engineering constraints. The devices that benefit most from d-tunable FP-BICs or narrow quasi-BICs are often also the most sensitive to gap nonuniformity, tilt, torsion, and lateral drift. Maintaining nanometer-scale spacing control and strict parallelism over a macroscopic optical aperture remains challenging, especially in MEMS/NEMS actuation where electrostatic pull-in, stiction, thermal drift, and actuator crosstalk can broaden, split, or destabilize high-Q resonances. Practical implementations will therefore likely require small active apertures, multi-actuator leveling, closed-loop optical or electrical feedback, or tiled architectures in which each unit maintains local control of the interlayer gap and alignment.

A related challenge is the gap between ideal theoretical designs and experimentally realized devices. Many predicted bilayer and moiré flat-optics effects rely on perfect periodicity, large numbers of moiré supercells, uniform interlayer spacing, and negligible material loss. In experiments, finite aperture, edge leakage, roughness, hole-size disorder, twist-angle error, gap nonuniformity, and layer-to-layer tilt can broaden or split high-Q resonances and obscure ideal BIC or flat-band behavior. The challenge is even more severe in plasmonic platforms, where Ohmic loss competes with radiative coupling and often requires gain to reveal collective lattice effects. For active, nonlinear, or quantum devices, additional constraints arise from emitter placement, gain uniformity, heat dissipation, and spectrum matching between emitters and cavity modes. Future progress will therefore require not only improved nanofabrication and alignment, but also standardized experimental extraction of Q, mode volume, radiation directionality, and disorder tolerance in the same device.

Beyond static control, bilayer and multilayer flat optics naturally interface with emerging concepts in adaptive

and intelligent photonics. Coupling reconfigurable multilayer structures with feedback, optimization algorithms, or machine-learning-based control could enable adaptive optical elements that respond autonomously to changing environments or tasks. From a functionality standpoint, multilayer architectures open new opportunities for nonlinear and quantum photonics, where layer-by-layer phase engineering, flatband-enhanced DOS, and controllable BIC singularities can be harnessed to design efficient sources of structured light, entangled photons, and nonclassical states. More broadly, the interlayer degrees of freedom as synthetic dimensions suggest connections to higher-dimensional topological physics and non-Hermitian photonic systems that remain largely unexplored.

Acknowledgements
H.T. acknowledges support from SONY Research Award Program. S. F. acknowledges the support by a MURI grant from the U.S. Air Force Office of Scientific Research (Grants No. FA9550-21-1-0312). HSN acknowledges support from the French National Research Agency (ANR) through the grants STRONG-NANO (ANR-22-CE24-0025), POLAROID (ANR-24-CE24-7616-01), SUPER-HERO (ANR-25-CE24-4066), and CHOCOLAT (ANR-25-CE47-6432). J.Y. acknowledges the support from the Heising-Simons Faculty Fellowship. Y.C. acknowledges support from the U.S. Department of Energy (Grant No. DE-SC0026044).

Author contributions
H.T. conceived the review and wrote the initial draft. H.T., S.F., J.Y., H.S.N., E.M., and Y.C. contributed to the organization, literature analysis, critical discussion, and revision of the manuscript. All authors reviewed and approved the final manuscript.

Data availability
No datasets were generated or analyzed during the current review article. All data discussed in this review are available from the cited publications.

Declarations

Competing interest
The authors declare no competing financial interests.

Received: 30 March 2026 Revised: 25 May 2026 Accepted: 25 May 2026
Published online: 09 July 2026

References

1. S. Fan, J.D. Joannopoulos, Analysis of guided resonances in photonic crystal slabs. Phys. Rev. B Condens. Matter **65**, 235112 (2002)
2. K. Shastri, F. Monticone, Nonlocal flat optics. Nat. Photonics **17**, 36 (2022)
3. J.D. Joannopoulos, S.G. Johnson, J.N. Winn, R.D. Meade, *Photonic Crystals: Molding the Flow of Light—Second Edition* (Princeton University Press, 2011)
4. C.W. Hsu, B. Zhen, A.D. Stone, J.D. Joannopoulos, M. Soljačić, Bound states in the continuum. Nat. Rev. Mater. **1**, 1 (2016).
5. S.G. Johnson, S. Fan, P.R. Villeneuve, J.D. Joannopoulos, L.A. Kolodziejski, Guided modes in photonic crystal slabs. Phys. Rev. B **60**, 5751 (1999)
6. K.V. Semushev, Z. Zhao, A. Proskurin, M. Song, X. Liu, M.V. Rybin, E.E. Maslova, A.A. Bogdanov, Robustness of bound states in the continuum in bilayer structures against symmetry breaking. Phys. Rev. Appl. **25**, 014038 (2026).
7. B. Zhen, C.W. Hsu, L. Lu, A.D. Stone, M. Soljačić, Topological nature of optical bound states in the continuum. Phys. Rev. Lett. **113**, 257401 (2014)
8. W. Suh, Z. Wang, S. Fan, Temporal coupled-mode theory and the presence of non-orthogonal modes in lossless multimode cavities. IEEE J. Quantum Electron. **40**, 1511–1518 (2004)
9. X. Ni, Y. Liu, B. Lou, M. Zhang, E.L. Hu, S. Fan, E. Mazur, H. Tang, Three-dimensional reconfigurable optical singularities in bilayer photonic crystals. Phys. Rev. Lett. **132**, 073804 (2024)
10. H. Son, T. Choi, K. Kim, Y. Kim, J. Bang, S.-J. Kim, B. Lee, Y. Jeong, Strong coupling induced bound states in the continuum in a hybrid metal–dielectric bilayer nanograting resonator. ACS Photonics **11**, 3221 (2024)
11. J. Tan, R. Pan, Y. Xiang, Z. Tang, B. Wang, J. Li, Unilateral asymmetric radiation in bilayer metasurfaces. Adv. Funct. Mater. **5**(28), 2501156 (2025)
12. H. Tang, F. Du, S. Carr, C. DeVault, O. Mello, E. Mazur, Modeling the optical properties of twisted bilayer photonic crystals. Light Sci. Appl. **10**, 157 (2021)
13. B. Wang, R. Pan, L. Yang, X. Ji, H. Yang, J. Li, Destructive interference mediated topological transitions in bilayer metasurfaces. Phys. Rev. Lett. **136**, 043801 (2026)
14. T. Fu, X. Gao, G. Xiao, T. Sun, Q. Li, F. Zhang, Y. Chen, H. Li, Z.-L. Deng, Superlattice bilayer metasurfaces simultaneously supporting electric and magnetic Fano resonances. Opt. Mater. Express **9**, 944 (2019)
15. G. Alagappan, F.J. García-Vidal, C.E. Png, Fabry-Perot resonances in bilayer metasurfaces. Phys. Rev. Lett. **133**, 226901 (2024)
16. M. Zhou, M. Liu, X. Qi, Y. Jiao, Enhancing second harmonic generation by merging symmetry-protected BIC and Fabry-Pérot BIC. Appl. Opt. **64**, 6984 (2025)
17. X. Zong, L. Li, Y. Liu, Merging bound states in the continuum in all-dielectric metasurfaces for ultrahigh-Q resonances. Opt. Lett. **48**, 5045 (2023)
18. Q.M. Ngo, K.Q. Le, D.L. Vu, V.H. Pham, Optical bistability based on Fano resonances in single- and double-layer nonlinear slab waveguide gratings. J. Opt. Soc. Am. B **31**, 1054 (2014)
19. A. Canós Valero, Z. Sztranyovszky, E.A. Muljarov, A. Bogdanov, T. Weiss, Exceptional bound states in the continuum. Phys. Rev. Lett. **134**, 103802 (2025)
20. X. Letartre, S. Mazauric, S. Cueff, T. Benyattou, H.S. Nguyen, P. Viktorovitch, Analytical non-Hermitian description of photonic crystals with arbitrary lateral and transverse symmetry. Phys. Rev. A (Coll. Park.) **106**, 033510 (2022)
21. Z. Yuan, V. Valuckas, Y. Wang, T. T. H. Do, N. Nie, Y.-C. Chen, H. S. Nguyen, C. Dang, and S. T. Ha, Topology-enabled switchable unidirectional radiative band in a bilayer photonic crystal, http://arxiv.org/abs/2602.11928.
22. Y. Shuai, D. Zhao, Z. Tian, J.-H. Seo, D.V. Plant, Z. Ma, S. Fan, W. Zhou, Double-layer Fano resonance photonic crystal filters. Opt. Express **21**, 24582 (2013)
23. Y.-C. Shuai, D. Zhao, Y. Liu, C. Stambaugh, J. Lawall, W. Zhou, Coupled bilayer photonic crystal slab electro-optic spatial light modulators. IEEE Photonics J. **9**, 1 (2017)
24. Y. Zhou, I.I. Kravchenko, H. Wang, H. Zheng, G. Gu, J. Valentine, Multifunctional metaoptics based on bilayer metasurfaces. Light Sci. Appl. **8**, 80 (2019)
25. W. Suh, M.F. Yanik, O. Solgaard, S. Fan, Displacement-sensitive photonic crystal structures based on guided resonance in photonic crystal slabs. Appl. Phys. Lett. **82**, 1999 (2003)
26. Y. Zeng, G. Hu, K. Liu, Z. Tang, C.-W. Qiu, Dynamics of topological polarization singularity in momentum space. Phys. Rev. Lett. **127**, 176101 (2021)
27. Y.-T. Fang, X. Qin, G. Zhang, S. He, Dynamical evolution of BIC-Fano dual modes under misalignment of two waveguide-coupled gratings. Laser Photonics Rev. **20**, e00341 (2026)
28. Z.-P. Zhuang, H.-L. Zeng, X.-D. Chen, X.-T. He, J.-W. Dong, Topological nature of radiation asymmetry in bilayer metagratings. Phys. Rev. Lett. **132**, 113801 (2024)
29. Y. Shuai, D. Zhao, A.S. Chadha, J.-H. Seo, H. Yang, S. Fan, Z. Ma, W. Zhou, Coupled double-layer Fano resonance photonic crystal filters with lattice-displacement. Appl. Phys. Lett. **103**, 241106 (2013)

30. S. Choudhary, R.W. Boyd, J.E. Sipe, Dark and bright modes, and their coherent control in dipolar metasurface bilayers. Phys. Rev. A **107**, 023521 (2023)
31. K.Y. Lee, K.W. Yoo, F. Monticone, J.W. Yoon, Dirac bilayer metasurfaces as an inverse Gires-Tournois etalon. Phys. Rev. Res. (2025). https://doi.org/10.1103/3dw5-nvdq
32. D. Choi, K.Y. Lee, D.-J. Shin, J.W. Yoon, S.-H. Gong, Unidirectional guided resonance continuum of Dirac bands in WS2 bilayer metasurfaces. Nat. Nanotechnol. (2025). https://doi.org/10.1038/s41565-025-01945-w
33. X. Yin, T. Inoue, C. Peng, S. Noda, Topological unidirectional guided resonances emerged from interband coupling. Phys. Rev. Lett. **130**, 056401 (2023)
34. Y. Zheng, H. BaratiSedeh, Y. Ji, L. Feng, M. Vincenti, M. Scalora, N. Litchinitser, Bilayer optical metasurfaces with multiple broken symmetries for nonlinear wavelength generation. Npj Metamater. **2**, 6 (2026)
35. Z.-P. Zhuang, X. Zhou, H.-L. Zeng, M.-Y. Li, Z.-M. Chen, X.-T. He, X.-D. Chen, L. Zhou, J.-W. Dong, Overcoming intrinsic dispersion locking for achieving spatio-spectral selectivity with misaligned bilayer metagratings. eLight (2025). https://doi.org/10.1186/s43593-025-00092-y
36. Y. Zhou, R. Zou, J. Zhan, Y. Wang, D. Dai, P.K. Choudhury, A. Forbes, Y. Ma, Quasi-bound states in the continuum on dislocated bilayer metal gratings for spatiotemporal vortex pulse generation. Laser Photonics Rev. (2025). https://doi.org/10.1002/lpor.202401391
37. K.Y. Lee, K.W. Yoo, S. Cheon, W.-J. Joo, J.W. Yoon, S.H. Song, Synthetic topological nodal phase in bilayer resonant gratings. Phys. Rev. Lett. **128**, 053002 (2022)
38. D.-H.-M. Nguyen, C. Devescovi, D.X. Nguyen, H.S. Nguyen, D. Bercioux, Fermi arc reconstruction in synthetic photonic lattice. Phys. Rev. Lett. **131**, 053602 (2023)
39. D.-H.-M. Nguyen, D.X. Nguyen, H.C. Nguyen, T. Louvet, E. Drouard, X. Letartre, D. Bercioux, H.S. Nguyen, Topological lasing from thouless pumping in bilayer photonic crystal. ACS Photonics (2026). https://doi.org/10.1021/acsphotonics.5c02664
40. J.-H. Park, A. Ndao, W. Cai, L. Hsu, A. Kodigala, T. Lepetit, Y.-H. Lo, B. Kanté, Symmetry-breaking-induced plasmonic exceptional points and nanoscale sensing. Nat. Phys. **16**, 462 (2020)
41. H. Tang, X. Ni, F. Du, V. Srikrishna, E. Mazur, On-chip light trapping in bilayer moiré photonic crystal slabs. Appl. Phys. Lett. (2022). https://doi.org/10.1063/5.0105365
42. S.M. Trushin, T. Ito, Y. Ishii, S. Iwamoto, Y. Ota, Flatband localization in 1D moiré bilayer photonic crystals with staggered potential. Opt. Lett. **50**, 2405 (2025)
43. P. Hong, Y. Liang, Z. Chen, G. Zhang, Robust moiré flatbands within a broad band-offset range. Adv. Photonics Nexus **2**, 066001 (2023)
44. Q. Jing, Z. Che, S. Chen, T. Xue, J. Wang, W. Liu, Y. Dai, L. Shi, J. Zi, Observation of Bloch flatbands and localized states in moiré bilayer grating. Nano Lett. **25**, 12118 (2025)
45. C. Saadi, S. Cueff, L. Ferrier, A. Benamrouche, M. Gayrard, E. Drouard, X. Letartre, H.S. Nguyen, S. Callard, Tailoring flatband dispersion in bilayer moiré photonic crystals. Laser Photonics Rev. **19**, e01038 (2025)
46. D.X. Nguyen, X. Letartre, E. Drouard, P. Viktorovitch, H.C. Nguyen, H.S. Nguyen, Magic configurations in moiré superlattice of bilayer photonic crystals: almost-perfect flatbands and unconventional localization. Phys. Rev. Research **4**, L032031 (2022)
47. Y. Lai, S. Pirotta, G. Urbinati, D. Gerace, M. Minkov, V. Savona, A. Badolato, M. Galli, Genetically designed L3 photonic crystal nanocavities with measured quality factor exceeding one million. Appl. Phys. Lett. **104**, 241101 (2014)
48. P. Hong, L. Xu, C. Ying, M. Rahmani, Flatband mode in photonic moiré superlattice for boosting second-harmonic generation with monolayer van der Waals crystals. Opt. Lett. **47**, 2326 (2022)
49. C. Saadi, H.S. Nguyen, S. Cueff, L. Ferrier, X. Letartre, S. Callard, How many supercells are required for unconventional light confinement in moiré photonic lattices? Optica **11**, 245 (2024)
50. P. Hong, M. Yi, L. Zhang, Y. Liang, High-quality flatband resonances in few-cell Moiré superlattices by band-offset tuning. Appl. Phys. Lett. (2024). https://doi.org/10.1063/5.0200219
51. W. Wang, W. Gao, X. Chen, F. Shi, G. Li, J. Dong, Y. Xiang, S. Zhang, Moiré fringe induced gauge field in photonics. Phys. Rev. Lett. **125**, 203901 (2020)
52. B. Lou, N. Zhao, M. Minkov, C. Guo, M. Orenstein, S. Fan, Theory for twisted bilayer photonic crystal slabs. Phys. Rev. Lett. **126**, 136101 (2021)
53. H. Tang, B. Lou, F. Du, M. Zhang, X. Ni, W. Xu, R. Jin, S. Fan, E. Mazur, Experimental probe of twist angle–dependent band structure of on-chip optical bilayer photonic crystal. Sci. Adv. **9**, eadh8498 (2023)
54. B. Lou, B. Wang, J.A. Rodríguez, M. Cappelli, S. Fan, Tunable guided resonance in twisted bilayer photonic crystal. Sci. Adv. **8**, eadd4339 (2022)
55. N.S. Salakhova, I.M. Fradkin, S.A. Dyakov, N.A. Gippius, Twist-tunable Moiré optical resonances. Phys. Rev. B. (2023). https://doi.org/10.1103/PhysRevB.107.155402
56. Y.-M. Liu, S.-K. Lin, P.-S. Li, Y.-R. Hao, and B. Yang, *Twisted Bi-Layer Magnetic Photonic Crystals*, http://arxiv.org/abs/2510.07714.
57. S. Xu, D. Wang, and R. Agarwal, *General Framework for Twisted Bilayer Photonic Crystal with Interlayer Coupling and Far-Field Response*, http://arxiv.org/abs/2509.23952.
58. H. Tang et al., An adaptive Moiré sensor for spectro-polarimetric hyperimaging. Nat. Photonics (2025). https://doi.org/10.1038/s41566-025-01650-z
59. J. He, S. Murai, T.Y. Lo, K. Tanaka, Alignment-free bilayer moiré metasurfaces with tunable twist angles. ACS Photonics **12**, 4608 (2025)
60. H. Zhou, X. Ni, B. Lou, S. Fan, Y. Cao, H. Tang, Control of chirality and directionality of nonlinear metasurface light source via moiré engineering. Phys. Rev. Lett. **134**, 043801 (2025)
61. Y. Wang, J. Xu, N. Liu, X. Liao, Z. Zhu, W. Xu, K. Liu, Ultrathin twisted bilayer photonic crystal with tunable micron-level near-field coupling for multimode polarization manipulation. Nano Lett. **25**, 10017 (2025)
62. Z. Wu, X. Chen, M. Wang, J. Dong, Y. Zheng, High-performance ultrathin active chiral metamaterials. ACS Nano **12**, 5030 (2018)
63. Z. Wu, Y. Liu, E.H. Hill, Y. Zheng, Chiral metamaterials via Moiré stacking. Nanoscale (2018). https://doi.org/10.1039/C8NR04352C
64. Z. Jiang, Z. Sun, Z. Gan, C. Liang, R. Qin, S. Zhang, W.-D. Li, Chiral emission from twisted Moiré metasurfaces with emissive gap layer. Laser Photonics Rev. (2025). https://doi.org/10.1002/lpor.202501633
65. Z. Wu, Y. Zheng, Moiré chiral metamaterials. Adv. Opt. Mater. **5**, 1700034 (2017)
66. D. Choi, S.-J. Lee, S.-W. Cho, C. B. Bark, S. Pak, D.-J. Shin, M. J. Park, and S.-H. Gong, *Strong Interlayer Coupling and Chiral Flat-Band Cascades in Twisted Bilayer Gratings*, http://arxiv.org/abs/2510.07381.
67. F. Du, H. Tang, Y. Liu, M. Zhang, B. Lou, G. Gao, X. Li, A. Enriquez, S. Fan, E. Mazur, Dynamic control of intrinsic optical chirality via MEMS-integrated photonic crystals. Optica (2026). https://doi.org/10.1364/optica.578880
68. E.S. Vyatkin, A.V. Poshakinskiy, S.A. Tarasenko, Emergent spin and orbital angular momentum of light in twisted photonic bilayer. Phys. Rev. B **111**, 125303 (2025)
69. M. Wang, N. Lv, Z. Zhang et al., Chiral orbital lasing in a twisted bilayer metasurface. Nat. Commun. **17**, 2369 (2026)
70. T. Zhang, K. Dong, J. Li, F. Meng, J. Li, S. Munagavalasa, C.P. Grigoropoulos, J. Wu, J. Yao, Twisted moiré photonic crystal enabled optical vortex generation through bound states in the continuum. Nat. Commun. **14**, 6014 (2023)
71. L. Huang, W. Zhang, X. Zhang, Moiré quasibound states in the continuum. Phys. Rev. Lett. **128**, 253901 (2022)
72. T. Zhang et al., *Moire-Enabled Optical Vortex with Tunable Topological Charge in Twisted Bilayer Photonic Crystals*, https://doi.org/10.48550/arXiv.2510.25214.
73. L. Qu, W. Wu, D. Zhang, C. Wang, L. Bai, C. Li, W. Cai, M. Ren, A. Alù, J. Xu, Beam shaping by stacked nonlinear moiré metasurfaces. Nano Lett. **25**, 4854 (2025)
74. N. Mou et al., Gradient moiré perovskite superlattices for laser beam steering. Sci. Adv. **11**, eadz8028 (2025)
75. S. Liu, S. Ma, R. Shao, L. Zhang, T. Yan, Q. Ma, S. Zhang, T.J. Cui, Moiré metasurfaces for dynamic beamforming. Sci. Adv. **8**, eabo1511 (2022)
76. B. Lou, H. Tang, F. Du, G. Gao, E. Mazur, S. Fan, Free-space beam steering with twisted bilayer photonic crystal slabs. ACS Photonics (2024). https://doi.org/10.1021/acsphotonics.4c00736
77. N. Roy, B. Lou, S. Fan, A. Mayer, M. Lobet, Twist-induced beam steering and blazing effects in photonic crystal devices. Light Sci. Appl. **14**, 263 (2025)

78. J. Guan, J. Hu, Y. Wang, M.J.H. Tan, G.C. Schatz, T.W. Odom, Far-field coupling between moiré photonic lattices. Nat. Nanotechnol. (2023). https://doi.org/10.1038/s41565-023-01320-7
79. K. Dong, T. Zhang, J. Li, Q. Wang, F. Yang, Y. Rho, D. Wang, C.P. Grigoropoulos, J. Wu, J. Yao, Flat bands in magic-angle bilayer photonic crystals at small twists. Phys. Rev. Lett. **126**, 223601 (2021)
80. L. Spencer et al., A Van der Waals moiré bilayer photonic crystal cavity. Nano Lett. **25**, 14459 (2025)
81. S. Yang, X. Zhao, X. Fu, W. Kong, K. Zhang, Flatbands in a bilayer surface plasmon crystal at a large twist angle due to interlayer strong coupling. Opt. Lett. **49**, 4334 (2024)
82. F. Wong, M. Cotrufo, Reconfigurable analog computation with twisted metasurfaces. Adv. Opt. Mater. (2025). https://doi.org/10.1002/adom.202502326
83. Y. Liu, C. Ouyang, Q. Xu, J. Ma, Y. Li, J. Han, W. Zhang, Magnetic moiré effects and two types of topological transition in a twisted-bilayer hyperbolic metasurface with double-split ring arrays. Opt. Express **30**, 36552 (2022)
84. X.-R. Mao, Z.-K. Shao, H.-Y. Luan, S.-L. Wang, R.-M. Ma, Magic-angle lasers in nanostructured moiré superlattice. Nat. Nanotechnol. **16**, 1099 (2021)
85. A. Raun, H. Tang, X. Ni, E. Mazur, E.L. Hu, GaN magic angle laser in a merged moiré photonic crystal. ACS Photonics **10**, 3001 (2023)
86. F.M. Fasanelli, F. Freire-Fernández, T.W. Odom, Symmetry-determined lasing from incommensurate moiré nanoparticle lattices. Adv. Opt. Mater. (2024). https://doi.org/10.1002/adom.202400797
87. M.J.H. Tan, F. Freire-Fernández, T.W. Odom, Symmetry-guided engineering of polarization by 2D moiré metasurfaces. ACS Nano **18**, 23181 (2024)
88. Y.-H. Ouyang, H.-Y. Luan, Z.-W. Zhao, W.-Z. Mao, R.-M. Ma, Singular dielectric nanolaser with atomic-scale field localization. Nature (2024). https://doi.org/10.1038/s41586-024-07674-9
89. H.-Y. Luan, Y.-H. Ouyang, Z.-W. Zhao, W.-Z. Mao, R.-M. Ma, Reconfigurable moiré nanolaser arrays with phase synchronization. Nature **624**, 282 (2023)
90. R.-M. Ma, H.-Y. Luan, Z.-W. Zhao, W.-Z. Mao, S.-L. Wang, Y.-H. Ouyang, Z.-K. Shao, Twisted lattice nanocavity with theoretical quality factor exceeding 200 billion. Fundam. Res. **3**, 537 (2023)
91. W.-Z. Mao, H.-Y. Luan, R.-M. Ma, Singulonics: narwhal-shaped wavefunctions for sub-diffraction-limited nanophotonics and imaging. eLight **5**, 27 (2025)
92. T. Ning, L. Zhao, Y. Huo, Y. Cai, Y. Ren, Giant enhancement of second harmonic generation from monolayer 2D materials placed on photonic moiré superlattice. Nanophotonics **12**, 4009 (2023)
93. X. Wang, Z. Liu, B. Chen, G. Qiu, D. Wei, J. Liu, Experimental demonstration of high-efficiency harmonic generation in photonic moiré superlattice microcavities. Nano Lett. **24**, 11327 (2024)
94. Y.-T. Wang et al., Moiré cavity quantum electrodynamics. Sci. Adv. **11**, eadv8115 (2025)
95. S. Yan et al., Cavity quantum electrodynamics with moiré photonic crystal nanocavity. Nat. Commun. **16**, 4634 (2025)
96. N. Liu, H. Liu, S. Zhu, H. Giessen, Stereometamaterials. Nat. Photonics **3**, 157 (2009)
97. M. Decker, M. Ruther, C.E. Kriegler, J. Zhou, C.M. Soukoulis, S. Linden, M. Wegener, Strong optical activity from twisted-cross photonic metamaterials. Opt. Lett. **34**, 2501 (2009)
98. A.V. Rogacheva, V.A. Fedotov, A.S. Schwanecke, N.I. Zheludev, Giant gyrotropy due to electromagnetic-field coupling in a bilayered chiral structure. Phys. Rev. Lett. **97**, 177401 (2006)
99. X. Yin, M. Schäferling, B. Metzger, H. Giessen, Interpreting chiral nanophotonic spectra: the plasmonic Born-Kuhn model. Nano Lett. **13**, 6238 (2013)
100. K. Hannam, D.A. Powell, I.V. Shadrivov, Y.S. Kivshar, Broadband chiral metamaterials with large optical activity. Phys. Rev. B **89**, 125105 (2014)
101. M. Decker, R. Zhao, C.M. Soukoulis, S. Linden, M. Wegener, Twisted split-ring-resonator photonic metamaterial with huge optical activity. Opt. Lett. **35**, 1593 (2010)
102. M.K. Chen, J.C. Zhang, C.W. Leung, L. Sun, Y. Fan, Y. Liang, J. Yao, X. Liu, J. Yuan, Y. Xu, D.P. Tsai, S.W. Pang, Chiral-magic angle of nanoimprint metadevice. Nanophotonics **12**, 2479–2490 (2023)
103. K. Tanaka, D. Arslan, S. Fasold, M. Steinert, J. Sautter, M. Falkner, T. Pertsch, M. Decker, I. Staude, Chiral bilayer all-dielectric metasurfaces. ACS Nano **14**, 15926 (2020)
104. R. Zhao, L. Zhang, J. Zhou, T. Koschny, C.M. Soukoulis, Conjugated gammadion chiral metamaterial with uniaxial optical activity and negative refractive index. Phys. Rev. B **83**, 035105 (2011)
105. Y. Zhao, A.N. Askarpour, L. Sun, J. Shi, X. Li, A. Alù, Chirality detection of enantiomers using twisted optical metamaterials. Nat. Commun. **8**, 14180 (2017)
106. Y. Li, S. Han, Y. Ao, Extrinsic and intrinsic chiral dual bound states in the continuum with opposite circular dichroism supported by an all-dielectric metasurface. Opt. Lett. **50**, 5422 (2025)
107. D. Gromyko et al., Unidirectional chiral emission via twisted bi-layer metasurfaces. Nat. Commun. **15**, 9804 (2024)
108. A. Overvig, N. Yu, A. Alù, Chiral quasi-bound states in the continuum. Phys. Rev. Lett. **126**, 073001 (2021)
109. J. Feng, X. Wang, M. Zeng, L. Fan, L. Ma, Y. Ji, F. Fan, S. Chang, Dual-band quasi-bound states in the continuum with opposite circular dichroism supported by single metallic bilayer twisted metasurface. Adv. Opt. Mater. (2025). https://doi.org/10.1002/adom.202402856
110. H. Qin, Z. Su, M. Liu, Y. Zeng, M.-C. Tang, M. Li, Y. Shi, W. Huang, C.-W. Qiu, Q. Song, Arbitrarily polarized bound states in the continuum with twisted photonic crystal slabs. Light Sci. Appl. **12**, 66 (2023)
111. N. Liu, H. Guo, L. Fu, S. Kaiser, H. Schweizer, H. Giessen, Three-dimensional photonic metamaterials at optical frequencies. Nat. Mater. **7**, 31 (2008)
112. N. Liu, M. Hentschel, T. Weiss, A.P. Alivisatos, H. Giessen, Three-dimensional plasmon rulers. Science **332**, 1407 (2011)
113. Y. Zhao, M.A. Belkin, A. Alù, Twisted optical metamaterials for planarized ultrathin broadband circular polarizers. Nat. Commun. **3**, 870 (2012)
114. T. Stolt et al., Backward phase-matched second-harmonic generation from stacked metasurfaces. Phys. Rev. Lett. **126**, 033901 (2021)
115. X. Li, G. Rui, Q. Cui, J. He, C. Xu, B. Gu, Modulation of optical force by adjusting the distance between three-layer photonic crystal slabs. Opt. Commun. **574**, 131172 (2025)
116. P. Hong, C. Lu, Y. Wang, C. Liang, L. Zhang, P. Cheng, W. Cheng, M. Yi, Y. Liang, Hybrid Morié flatbands in triple-layer superlattices via flatbands coupling. Chaos Solitons Fractals **199**, 116598 (2025)
117. Q. Wang, Y. Li, S. Wang, S. Cao, X. Xu, and C. Qian, *Twisted Heterobilayer Photonic Crystal Based on Stacking and Selective Etching of 2D Materials*, http://arxiv.org/abs/2503.04366.
118. A.H. Dorrah, J.-S. Park, A. Palmieri, F. Capasso, Free-standing bilayer metasurfaces in the visible. Nat. Commun. **16**, 3126 (2025)
119. H. Tang, Y. Wang, X. Ni, K. Watanabe, T. Taniguchi, P. Jarillo-Herrero, S. Fan, E. Mazur, A. Yacoby, Y. Cao, On-chip multi-degree-of-freedom control of two-dimensional materials. Nature (2024). https://doi.org/10.1038/s41586-024-07826-x
120. X. Jing, N. Kroneberg, A. Peil, B. Renz, L. Ding, T. Heil, K. Hipp, P.A. van Aken, H. Yan, N. Liu, DNA moiré superlattices. Nat. Nanotechnol. **20**, 1464 (2025)